

Low-synchronization Arnoldi Methods for the Matrix Exponential with Application to Exponential Integrators

Tanya V. Tafolla, Stéphane Gaudreault, Mayya Tokman

October 22, 2024

Abstract

High order exponential integrators require computing linear combination of exponential like φ -functions of large matrices A times a vector v . Krylov projection methods are the most general and remain an efficient choice for computing the matrix-function-vector-product evaluation when the matrix is A is large and unable to be explicitly stored, or when obtaining information about the spectrum is expensive. The Krylov approximation relies on the Gram-Schmidt (GS) orthogonalization procedure to produce the orthonormal basis V_m . In parallel, GS orthogonalization requires *global synchronizations* for inner products and vector normalization in the orthogonalization process. Reducing the amount of global synchronizations is of paramount importance for the efficiency of a numerical algorithm in a massively parallel setting. We improve the parallel strong scaling properties of exponential integrators by addressing the underlying bottleneck in the linear algebra using low-synchronization GS methods. The resulting orthogonalization algorithms have an accuracy comparable to modified Gram-Schmidt yet are better suited for distributed architecture, as only one global communication is required per orthogonalization-step. We present geophysics-based numerical experiments and standard examples routinely used to test stiff time integrators, which validate that reducing global communication leads to better parallel scalability and reduced time-to-solution for exponential integrators.

1 Introduction

Many problems in science and engineering require simulating complex systems with dynamics governed by various forces acting over a wide range of time scales. Numerical solutions of such systems typically involve spatial discretization of the partial differential equations (PDEs) and their transformation into large systems of ordinary differential equations (ODEs) using the method of lines. Because these systems span wide temporal scales, the resulting ODEs are typically stiff, necessitating numerical solutions over intervals far exceeding the characteristic time scale of the fastest modes. Therefore, selecting an appropriate time integration method is crucial for ensuring both accuracy and efficiency in computing solutions.

Explicit time integrators are unsuitable for such problems due to strict stability limitations on the timestep and implicit methods are often the preferred choice. With implicit schemes, stiffness manifests in the increased computational complexity of both nonlinear and linear solvers involved in approximating solution at each timestep. A common numerical approach to implementing an implicit method is to use the Jacobian-Free Newton-Krylov algorithm [30]. In this method the

nonlinear system of equations resulting from the implicit discretization is handled with a Newton iteration which, in turn, involves solution of linear systems using Krylov subspace solvers. For stiff systems, the Krylov method can converge slowly, and a preconditioner is needed to make it efficient. However, constructing an effective preconditioner is often challenging and is the subject of considerable research.

Over the past decades, exponential integrators have emerged as an efficient alternative for numerically integrating large-scale stiff systems. Exponential time integrators express the numerical solution as a linear combination of products of exponential-like functions of the Jacobian, or its approximations, and vectors [33, 11, 55, 56, 26]. Similar to implicit methods, exponential schemes have good stability properties that allow integration with a large timestep. For problems where a fast preconditioner is not available, exponential methods can offer computational savings per timestep compared to implicit integrators [34, 56]. This is particularly true when Krylov-projection based algorithms are used for both implicit and exponential integrators. For many large-scale applications of interest, evaluating exponential-like functions of matrices can be more efficient and accurate than computing a rational function of a Jacobian, which is part of an implicit timestep [34].

The dominating cost of exponential integrators is the computation of the exponential-like φ -functions times a vector. Krylov methods have shown to be efficient for problems involving large matrices that are difficult to compute explicitly or store, or when obtaining information about the spectrum is prohibitively expensive [36]. The main idea of Krylov subspace methods is that matrix functions can be efficiently computed using a projection of the matrix onto a low-dimensional subspace. For the general case where the matrix is non-symmetric, this is generally accomplished through the Arnoldi iteration. At the base of the Arnoldi method is essentially a Gram-Schmidt orthogonalization process which requires a projection of consecutive Krylov vectors onto an orthogonal basis computed during previous iterations. Thus, the Arnoldi method does not scale well in parallel due to the cost of global communication needed to compute the inner products involved in the orthogonalization procedure. This global communication can become a bottleneck as the number of processors increases [2].

Various techniques have been proposed in recent work on the General Minimal Residual (GMRES) method to reduce global communication by reformulating the orthogonalization process into a projection onto the orthogonal complement [4, 51, 53]. Such algorithms aim to decrease the amount of the global communication required by the Arnoldi iteration to a single call per Arnoldi-step, improving the strong scaling properties of linear solvers on distributed memory parallel systems.

The aim of this paper is to explore Krylov methods that minimize global communication and to extend their application to computing the matrix exponential, with a primary focus on enhancing the overall performance of exponential time integrators. We demonstrate the performance advantages of the new methods using a variety of large-scale problems, including some standard benchmarks routinely used by the numerical weather prediction community [19, 58]. Our numerical experiments indicate that these low-synchronization orthogonalization methods are strong competitors to current techniques when using a large number of processors. The methods also exhibit a clear trend of improved strong scaling behavior as the number of processors increases, resulting in enhanced efficiency for exponential time integrators. The paper explores the potential of these methods to address the communication bottleneck and improve the overall performance of exponential integrators for large-scale simulations.

The remainder of this paper is organized as follows: Section 2 provides background information and highlights parallel scaling limitations. Section 3 presents current low-synchronization variants and introduces a new hybrid low-synchronization Arnoldi algorithm. Section 4 shows numerical evidence of the improvement in parallel scalability achieved by different exponential time integrators

when using low-synchronization Arnoldi methods. Finally, Section 5 draws conclusions and outlines future research directions.

2 Background and Motivation

Exponential time integrators are a family of numerical methods for solving initial value problems of the form

$$\frac{d}{dt}u(t) = F(u(t)), \quad u(0) = u_0, \quad u(t) \in \mathbb{R}^N \quad (1)$$

where $u(t)$ is the solution of (1) at time t , N is the number of degrees of freedom, and $F(u(t))$ is the forcing term. If the time interval $[t_0, t_{end}]$ is discretized over a set of nodes $\{t_n\}_{n=0}^M$, then the solution of (1) at time t_n is given by $u(t_n)$. Using Taylor expansion about the exact solution $u(t_n)$, the system (1) can be written as

$$\frac{du}{dt} = F(u(t_n)) + J(u(t_n))(u - u(t_n)) + R(u(t)), \quad (2)$$

where $J(u(t_n)) = \frac{\partial F}{\partial u}(u(t_n))$ is the Jacobian matrix, $F(u(t_n))$ is the right-hand side of (1) at time t_n , and $R(u(t)) = F(u(t)) - F(u(t_n)) - J(u(t_n))(u(t) - u(t_n))$ is the nonlinear remainder after two terms in the Taylor expansion. Employing $e^{-J_n t}$ as an integrating factor and integrating (2) exactly over the time interval $[t_n, t_{n+1}]$ yields the following Volterra integral equation

$$u(t_{n+1}) = u(t_n) + \varphi_1(hJ(u(t_n)))hF(u(t_n)) + \int_{t_n}^{t_{n+1}} e^{(t_{n+1}-t)J_n} R(u(t))dt, \quad (3)$$

where $\varphi_1(z) = (e^z - 1)/z$. Equation (3) is the starting point for deriving various exponential integrators by replacing the exact values with the numerical approximation, i.e. $u_n \approx u(t_n)$ or $J_n \approx \frac{\partial F}{\partial u}(u(t_n))$, and approximating the nonlinear integral in the right-hand-side to estimate u_{n+1} . For example, well-known quadratures that use either nodes t_i or successively computed approximations of the solution over the interval $[t_n, t_{n+1}]$ will result in the multistep- or Runge-Kutta-type integrators respectively [33, 55, 56]. Any such polynomial approximation of the nonlinear remainder function $R(u(t))$ will result in the approximate solution u_{n+1} being expressed as a linear combination of exponential-like φ -functions multiplied by vectors

$$\varphi_0(J_n)b_0 + \varphi_1(J_n)b_1 + \varphi_2(J_n)b_2 + \dots + \varphi_p(J_n)b_p \quad (4)$$

with the φ -functions defined as

$$\varphi_0(z) = e^z \quad (5)$$

$$\varphi_k(z) = \int_0^1 \frac{e^{(1-\theta)z}\theta^{k-1}}{(k-1)!} d\theta \quad \forall k \in \mathbb{N}^{>0}. \quad (6)$$

Evaluating linear combinations of the form (4) constitutes the main computational cost of exponential time integrators. Various approaches exist for computing the φ -functions, including Taylor series [1], Leja methods [9, 16], interpolation methods [8], and Krylov subspace methods [22, 31, 57]. We are interested in problems where matrix J_n is large, stiff and might not even be available explicitly. For example, F could be a result of a complex spatial discretization of the forcing terms

in a stiff system of PDEs and an explicit analytic evaluation of its Jacobian matrix might be completely impractical from the efficiency and memory storage perspectives. Often only a function that computes a product of the Jacobian matrix with a vector is provided. The most appropriate numerical approach to evaluate linear combinations (4) in such applications becomes the Krylov subspace projection-based methods. Improving parallel scalability of the Krylov projection is the focus of this paper.

2.1 Linear combination of φ -functions

To optimize evaluation of linear combinations of φ -functions and vectors we follow previous work [1, 22, 46] and reformulate the linear combination (4) as a single matrix exponential using the equivalence

$$\sum_{j=0}^p \tau^j \varphi_j(\tau J_n) v_j = (I_N \ 0) \exp(\tau A) \begin{pmatrix} v_0 \\ e_p \end{pmatrix}, \quad (7)$$

where the augmented matrix A is defined as

$$A = \begin{bmatrix} \tau J_n & B \\ 0 & K \end{bmatrix} \in \mathbb{R}^{(N+p) \times (N+p)}, \quad (8)$$

$$B = [b_p, \dots, b_1] \in \mathbb{R}^{N \times p}, \quad K = \begin{bmatrix} 0 & I_{p-1} \\ 0 & 0 \end{bmatrix} \in \mathbb{R}^{p \times p}, \quad \tau \in \mathbb{R}, \quad (9)$$

and e_p is the p th column of I_p , the identity matrix of size p .

In order to match the linear combination of the general ansatz (4), the exponential of the augmented matrix must be computed with $\tau = 1$. It is important to note that assembling the augmented matrix A is not required; instead, the implementation of this technique only necessitates the product of J_n with a vector of compatible dimension. The task now is to consider how the exponential of the augmented matrix can be efficiently evaluated using a Krylov subspace method.

2.2 Krylov Subspace Approximation

Krylov subspace approximations of the products of matrix functions and vectors of type $f(A)b$ are based on the projection of matrix $A \in \mathbb{R}^{d \times d}$ and nonzero vector $b \in \mathbb{R}^d$ onto a smaller Krylov subspace of dimension $m \ll d$,

$$\mathcal{K}_m(A, b) = \text{span}\{b, Ab, A^2b, \dots, A^{m-1}b\}. \quad (10)$$

In the most general case, when A is a non-symmetric matrix, the Arnoldi process is employed to compute the Hessenberg reduction

$$H_m = V_m^T A V_m, \quad (11)$$

where $V_m = [v_1, \dots, v_m]$ is a matrix whose columns form an orthonormal basis of \mathcal{K}_m , and $H_m \in \mathbb{R}^{m \times m}$ is upper Hessenberg. Gram-Schmidt algorithm is commonly used as part of the Arnoldi process to generate a set of orthonormal vectors $\{v_1, v_2, \dots, v_{m+1}\}$. Note that the matrix $V_m^T V_m$ is the identity when the basis $\{v_1, v_2, \dots, v_{m+1}\}$ is orthonormal. This property can be used to assess the departure from orthogonality in the numerical algorithms. In matrix form Arnoldi iteration can be written as

$$A V_m = V_m H_m + h_{m+1,m} v_{m+1} e_m^T, \quad (12)$$

where e_m is the m th unit vector. Using Krylov projection the matrix exponential can be approximated as

$$e^A b \approx \|b\|_2 V_m e^{H_m} e_1. \quad (13)$$

The magnitude of the error associated with first evaluating the matrix exponential function on the smaller Krylov subspace $\mathcal{K}_m(A, b)$ and expanding the result back to the original space \mathbb{R}^N is significant when $\|A\|_2$ is large (see, e.g., Theorem 4.3 in [44]). Thus, the convergence of the Krylov iteration is slow when A is stiff. A common strategy to mitigate these issues is to use adaptive sub-stepping, analogous to the techniques used in many solvers for ordinary differential equations [22, 37, 46, 57]. The basic idea, exemplified here for the computation of $w(\tau_{i+1}) = e^{\tau_i A} w(\tau_i)$, is to solve an equivalent linear initial value problem

$$\frac{d}{dt} w(\tau) = Aw(\tau), \quad w(0) = b. \quad (14)$$

The action of the matrix exponential is obtained through the recurrent evaluation of the solution to this initial value problem, referred to as sub-stepping

$$e^{\tau A} b = e^{(\tau_n + \dots + \tau_2 + \tau_1) A} b \quad (15a)$$

$$= e^{\tau_n A} (\dots (e^{\tau_2 A} (e^{\tau_1 A} b))), \quad (15b)$$

where each product $e^{\tau_i A} b_{\tau_i}$ in (15b) is approximated with a Krylov projection (13).

This sub-stepping procedure reduces the norm of the matrix and speeds up convergence of the Krylov iteration. At each sub-step, both the size τ_i and Krylov subspace dimension m_i are selected adaptively as in [22], and a maximum threshold on m_i is set based on the characteristics of the hardware.

2.3 Parallel scaling limitations of the Krylov subspace projection

As outlined above, the sub-stepping procedure requires an Arnoldi iteration to be performed at each substep τ_i . The overall computational cost of an exponential time integrator that utilizes the Krylov subspace projections to evaluate linear combinations (4) is then primarily dependent on the efficiency of the underlying Arnoldi iterations. Using this algorithm on a distributed memory computational platform usually assumes that vector entries are distributed among P processors. Some computations such as vector scaling or vector addition can be done locally by each individual processor. However, other computations such as inner products require global communication. Each processor handles its respective portion, then the intermediate results are shared among the remaining processors, added through global communication, and broadcasted back to each processor, for instance in the form of a `MPI_Allreduce` call¹.

The primary challenge in implementing the Arnoldi process for parallel computational platforms lies in the Gram-Schmidt orthogonalization. Two common methods for orthogonalization are Modified Gram-Schmidt (MGS) and Classical Gram-Schmidt (CGS). Although CGS requires only two global communication calls at each j^{th} Arnoldi step (one for all the inner products and one for vector normalization), this algorithm is less stable and more susceptible to rounding errors compared to MGS. MGS is a more stable algorithm, but is significantly more expensive in

¹The `MPI_Allreduce` function of the Message Passing Interface (MPI) is a collective communication operation that performs a global reduction operation (for example a summation) on a set of input values and distributes the result to all participating processes. This function is blocking and introduces collective synchronization into the exponential solver.

parallel, requiring $(j + 1)$ global communications (j inner products and one for vector normalization, see Algorithm 1) at the j^{th} Arnoldi step. For efficient Krylov-projection approximation of $e^{\tau_i A} b_i$ it is therefore desirable to develop an algorithm that reduces the total global communication during the orthogonalization process without compromising the stability and the accuracy of the approximation.

Algorithm 1 Arnoldi proces (with modified Gram-Schmidt)

```

1: procedure ARNOLDI( $A, b, m$ )                                ▷ matrix, initial vector, size of subspace
2:    $\beta = \|b\|_2$ 
3:    $v_1 = b/\beta$ 
4:    $j = 0$ 
5:   while  $j < m$  do
6:      $j = j+1$ 
7:      $v_{j+1} = Av_j$                                           ▷ next vector in basis
8:     for  $i = 1 \dots j$  do                                    ▷ orthogonalization
9:        $H_{ij} = v_i^T v_{j+1}$                                     ▷ global sync
10:       $v_{j+1} = v_{j+1} - H_{ij}v_i$ 
11:       $\text{nrm} = \|v_{j+1}\|_2$                                   ▷ global sync
12:      if  $\text{nrm} \approx 0$  then                                  ▷ check for lucky breakdown[32]
13:        break
14:       $v_{j+1} = v_{j+1}/\text{nrm}$ 
15:       $H_{j+1,j} = \text{nrm}$ 

```

2.3.1 Incomplete orthogonalization process

One way to reduce the total amount of global communication is the Incomplete Orthogonalization Process (IOP), in which new vectors are orthogonalized relative to a few previous basis vectors, e.g., the previous two, as opposed to all of them. Incomplete orthogonalization was previously used for solving linear systems and eigenvalue problems [42, 43] and has since been extended to matrix exponential computations [22, 31, 57].

While the IOP seems to improve overall parallel scalability and works well in many practical applications (e.g. [21]), its behavior is difficult to analyze. In contrast with the standard Arnoldi procedure, the IOP produces a H_m which is not Hessenberg, the columns of V_m do not form an orthonormal basis and $V_m^T V_m$ is not the identity matrix. Furthermore, in theory, rounding errors can result in basis vectors that are nearly collinear with those not orthogonalized, potentially compromising the accuracy of the approximation (13). In some applications IOP does not produce sufficient accuracy and full orthogonalization is required [50]. Thus, it is desirable to develop a Krylov method that uses complete orthogonalization that can be efficiently scaled for parallel computing platforms.

For our study, we use the KIOPS algorithm, a Krylov Incomplete Orthogonalization Procedure developed by Gaudreault et al. that combines incomplete orthogonalization (orthogonalizing against the previous two vectors) from [31, 57], substepping of $e^A v$, and Krylov adaptivity in Section 2.2 of the augmented matrix from Section 2.1. This algorithm has substepping and adaptivity techniques for τ_i and m_i that do not require multiplication with the matrix A and take into account the impact of round-off error, resulting in an overall highly efficient and accurate algorithm for computing $e^{\tau_i A} b_i$ [22]. This method was shown to improve the efficiency of exponential integrators for solving

commonly tested stiff PDEs and applications ranging from combustion to weather prediction [21, 22, 50]. The structure of the algorithm (further discussed in Section 4.1) also allows for easy comparisons of the orthogonalization schemes that will be presented in the following section.

3 Low-synchronization Arnoldi Algorithm for Krylov Approximations

Arnoldi algorithms are used for a wide variety of applications ranging from finding eigenvalues (and corresponding eigenvectors) [4, 25, 29] to solving linear systems $Ax = b$ with GMRES [51, 23, 4, 52, 59]. The parallel efficiency of these algorithms has been a subject of extensive interest and research, dating back to the mid 90's [45, 39, 13]. The most recent developments in improving the parallel scalability of Krylov linear solvers on massively parallel computing platforms have been focused on developing low-synchronization Arnoldi methods [4, 23, 51, 52, 59]. Low-synchronization methods aim to reduce the amount of global communication or synchronization points in an algorithm, such as `MPI_Allreduce` calls. Low-synchronization Arnoldi methods are derived by reformulating the orthogonalization process of Arnoldi algorithm to trade off increased computational complexity for reduced global communication needed at each Arnoldi step. In this study, we focus on Modified Gram-Schmidt variants of the low-synchronization methods that require one global synchronization per Arnoldi-step. We consider the `WY` methods from [51, 54] and the iterated Gauß-Seidel formulations [52]. These algorithms employ reformulation of the orthogonalization process in MGS by expressing it as the projection onto the orthogonal complement. The following sections describe the low-synchronization methods and their extension to exponential integrators.

3.1 Main ideas of low-synchronization methods

3.1.1 Projection onto the orthogonal complement

A key idea of many modern low-synchronization techniques is that the orthogonalization of each subsequent vector v_{j+1} in the Krylov basis at Arnoldi step j is done by projecting it onto the orthogonal complement of the j -dimensional Krylov subspace $V_j^\perp = \{w \in \mathbb{R}^n : \langle v, w \rangle = 0, \forall v \in V_j\}$ [41, 51]. The projection matrix onto V_j^\perp is given by

$$P = I_j - V_j(V_j^T V_j)^{-1} V_j^T \quad (16)$$

and v_{j+1} can be orthogonalized as follows

$$Pv_{j+1} = (I_j - V_j(V_j^T V_j)^{-1} V_j^T)v_{j+1} \quad (17)$$

where I_j is the $j \times j$ identity matrix. The sequential orthogonalization of the MGS algorithm (lines 8 - 10 of Algorithm 1) can then be replaced by a matrix-vector multiplication with the projection matrix P and vector v_{j+1} . The interior matrix $(V_j^T V_j)^{-1}$ can be used to correct for the non-orthogonality of the basis due to round-off errors in finite precision arithmetic; although the inner products $v_i^T v_j$ are expected to be small, they are not exactly zero.

The low-synchronization Arnoldi algorithms explored in this study are rooted in similar principles but differ in terms of possible loss of orthogonality and computational complexity that vary based on the distinct approximations to the correction matrix $T_j \approx (V_j^T V_j)^{-1}$. The different approaches to estimating the correction matrix T_j are discussed in the subsequent sections.

3.1.2 Lagged normalization

The second strategy used to minimize communication is lagged normalization [25, 29]. The key idea is to postpone the normalization of the next vector v_{j+1} until the communication needed for the norm can be grouped with other calculations such as inner products in the subsequent step. In this paper, we use low-synchronization methods each with their unique approximation to the orthogonal projector along with lagged normalization.

3.2 Hybrid low-synchronization

The lagged normalization strategy delays the normalization of vector v_{j+1} at Arnoldi step j . Grouping the computation of the norm for v_{j+1} at the next Arnoldi step with other inner products reduces the total amount of global communication to one per-Arnoldi-iteration, i.e. eliminating the global communication from the vector normalization. Although lagged normalization is essential for the orthogonal complement-based orthogonalization to remain a one-synchronization method, the vector v_{j+1} will potentially have a large norm. This will result in an unstable iteration when the matrix operator is applied to v_{j+1} .

An alternative would be to introduce a Pythagorean form of a norm estimate [23, 25]. At the end of each Arnoldi step j , the norm estimate of v_{j+1} can be computed and v_{j+1} can then be “normalized” using the following estimate [23, 25]:

$$\text{nrm} = \sqrt{\|v_{j+1}\|_2^2 - \sum_{i=0}^j (v_i^T v_{j+1})^2}. \quad (18)$$

The matrix operator applied to v_{j+1} at the subsequent iteration should then be stable. Furthermore, the inner products $V_{1:j+1}^T v_{j+1}$ required by the norm estimate (18) are obtained by the grouped communication from section 3.1.1 (details in sec. 3.2.1). Therefore, no additional communication is required, and the algorithm remains a one-synchronization method. However, this norm estimate is not exact for MGS and can be sensitive to round-off error if the terms inside the square root are similar in magnitude, i.e if orthogonality of V_m is lost [23]. This can cause the argument of the square root to become negative and the algorithm to break down. The inaccuracy of the norm estimate can also impact the accuracy of the Krylov projection since the norm values are entries of the Hessenberg matrix used in computing the projection of the matrix-exponential (eq. 13). Therefore, a combination of the orthogonal complement projection and norm estimate is also potentially unstable.

Given the instabilities of the orthogonal complement-based orthogonalization paired with either lagged normalization or the norm estimate, we present a hybrid version of low-synchronization algorithms that combines all three techniques (projection to the orthogonal complement, lagged normalization and norm estimate); an outline of the hybrid low-synchronization algorithm is presented in Algorithm 2. At the end of Arnoldi step j , the norm estimate of vector v_{j+1} is computed using equation (18), allowing for a stable matrix-vector product at the following step. At the next step, after the matrix-vector product to extend the Krylov basis, the vectors v_{j+1} and v_j (current and previous vector) are re-scaled by the norm-estimate of v_j , which was computed at the previous iteration ($V_{j:j+1} = \text{nrm_est} * V_{j:j+1}$). The re-scaling of v_j will ensure that the true norm is obtained from the group computation of inner products (details in sec. 3.2.1). The true norm of the previous vector is then used in the Hessenberg matrix, and to accurately normalize the previous vector. This new hybrid low-synchronization method requires only one global synchronization, avoids multiplying matrix A and vector v_j with a large norm and uses the true norm obtained from lagged

normalization, avoiding inaccuracies from finite precision stemming from the norm estimate. We call these methods “hybrid” because we incorporate lagged normalization and perform normalization at the end of each Arnoldi step.

Sections 3.2.1 to 3.2.3 expand on details regarding the grouped computation for obtaining all necessary terms (line 6, Algorithm 2), each low-synchronization method’s approximation to the correction matrix T (line 7, Algorithm 2), and the inclusion of the norm-estimate computation (line 5 and 9, Algorithm 2).

Algorithm 2 Outline of hybrid low-synchronization algorithm with techniques (sec. 3.1.1), (sec. 3.1.2), and norm estimate (eq. 18)

```

1: procedure HYBRID_LOWSYNC( $A, v_1, m$ )      ▷ matrix operator, initial vector, size of subspace
2:   for  $j = 1, \dots, m$  do
3:     Expand Krylov basis  $\{v_1, v_2, \dots\} : v_{j+1} = Av_j$ 
4:     if  $j > 1$  then
5:       Re-scale  $v_{j+1}$  and  $v_j$  by norm estimate:  $v_{j:j+1} = \mathbf{nrm\_est} \times v_{j:j+1}$ 
6:       Grouped computation for projection (17); includes lagg normalization and norm est (18).
7:       Formation of correction matrix  $T \approx (V^T V)^{-1}$ 
8:       Projection via (17)
9:       “Normalization” of  $v_{j+1}$  via (18)

```

3.2.1 Hybrid Compact WY MGS

Recall the orthogonalization for-loop in MGS (Algorithm 3), here the superscript indexing i is added to explicitly label v_{j+1} at the i^{th} step of the recursive orthogonalization.

Algorithm 3 Modified Gram-Schmidt Orthogonalization

```

1: procedure MGS_ORTHO( $A, b, m$ )
2:   for  $i = 1 \dots j$  do                                     ▷ orthogonalization
3:      $H_{ij} = v_i^T v_{j+1}^{(i)}$                                ▷ global sync
4:      $v_{j+1}^{(i+1)} = v_{j+1}^{(i)} - H_{ij} v_i$ 

```

If the for-loop is unrolled at iteration $i = j$, we can obtain an expression for $v_{j+1}^{(i+1)}$ in terms of $v_{j+1}^{(1)} = Av_j$. As an illustrative example, consider the for-loop expansion for $j = 2$ (orthogonalizing v_3 against v_1 and v_2)

$$v_3^{(3)} = v_3^{(2)} - \langle v_2, v_3^{(2)} \rangle v_2 \tag{19a}$$

$$v_3^{(3)} = v_3^{(1)} - \langle v_1, v_3^{(1)} \rangle v_1 - \langle v_2, v_3^{(1)} - \langle v_1, v_3^{(1)} \rangle v_1 \rangle v_2 \tag{19b}$$

The expansion (19b) can be simplified and re-written as the application of the rank-1 projectors $(I - v_j v_j^T) \dots (I - v_1 v_1^T) v_{j+1}$ [25, 51]. The product of these rank 1 projectors can then be expressed in matrix form as

$$(I - v_j v_j^T) \dots (I - v_1 v_1^T) = I - V_j T_j V_j^T. \tag{20}$$

The matrix form of the rank-1 projections (20) then forms an approximation to the orthogonal complement, with the lower triangular loss-of-orthogonality (or correction) matrix T_j approximating

the interior symmetric matrix of the projection $(V^T V)^{-1}$ from (16). The MGS-Arnoldi process is then re-written as a projection to the orthogonal complement through the application of (20) instead of the sequential for-loop from Algorithm 3. This re-formulation of the MGS-Arnoldi through the orthogonal complement is based on Ruhe [41], and has been recently extended by Świrydowicz et al. employing lagged normalization; we will refer to it as the *Compact WY* MGS (Algorithm 6 in [51]). The correction matrix T_j is computed one row at a time at each Arnoldi step j through the recursion formula

$$T_1 = [1] \tag{21a}$$

$$T_j = \begin{bmatrix} T_{j-1} & 0 \\ -(V_{j-1}^T v_j)^T T_{j-1} & 1 \end{bmatrix}. \tag{21b}$$

Through this re-formulation only one global reduction sum is needed at each Arnoldi step for the computation of $V_{1:j}^T V_{j:j+1}$ [51]. The resulting $(j \times 2)$ matrix is given by

$$\begin{bmatrix} v_1^T v_j & v_1^T v_{j+1} \\ v_2^T v_j & v_2^T v_{j+1} \\ \vdots & \vdots \\ v_j^T v_j & v_j^T v_{j+1} \end{bmatrix}. \tag{22}$$

After computation (22), we have all components necessary for the projection. The second column of (22) is $V_j^T v_{j+1}$ from the projection (17), the first $(j - 1)$ rows of column one are used for in the recursion formula for T_j (21b), and the square norm of the previous vector v_j is row j of column one.

However, in order to incorporate the norm estimate, $\|v_{j+1}\|_2^2$ is needed. Therefore, we extend the computation (22) to $V_{1:j+1}^T V_{j:j+1}$. This will result in a $(j + 1) \times 2$ matrix whose entries are given by

$$\begin{bmatrix} v_1^T v_j & v_1^T v_{j+1} \\ v_2^T v_j & v_2^T v_{j+1} \\ \vdots & \vdots \\ v_j^T v_j & v_j^T v_{j+1} \\ v_{j+1}^T v_j & v_{j+1}^T v_{j+1} \end{bmatrix}. \tag{23}$$

with the additional component of $\|v_{j+1}\|_2^2$ (row $(j + 1)$ of the second column) for the norm estimate.

Once (23) is calculated, the remaining steps for the orthogonalization are computing the local matrix-vector product in the recursion formula for T_j (21b) and the projection of v_{j+1} via equation (17). The values of the upper Hessenberg matrix $H_{1:j,j}$ are obtained by the local matrix-vector product $T_j V_j^T v_{j+1}$. At the end of the Arnoldi step, v_{j+1} is “normalized” using equation (18), and at the subsequent step, the computation Av_j should be stable. In order to then obtain the true norm of the previous vector from computation (23) (i.e. row j , column 1), vectors $V_{j:j+1}$ are re-scaled by the norm estimate (computed at the previous iteration) after the matrix-vector product Av_j is computed (see line 15 in Algorithm 4).

We refer to the combination of the one-synchronization version (projection with lagged normalization) with a norm estimate computation as the hybrid CWY algorithm (H-CWY). The algorithm for a general hybrid low-synchronization method is presented in Algorithm 4 with the corresponding technique for obtaining the correction matrix in Algorithm 5. The hybrid version remains a one-synchronization algorithm (line 13 of Algorithm 4 for the inner products of the grouped

communication) but at the cost of additional computation from the norm estimate and a larger communication for the additional row of $V^T V$.

3.2.2 Hybrid Neumann Series MGS

The CWY method requires two matrix-vector products with computational complexity of $\mathcal{O}(m^2)$, which results in a higher computational cost than MGS [51]. In order to reduce this computational cost, the alternative method *Truncated Neumann Series* MGS (NWY) presented by Thomas et al. (algorithm 4.1 in [54]) approximates the correction matrix T with a finite Neumann series

$$T_m = (I + L_m)^{-1} = I - L_m + L_m^2 - \dots + L_m^p \quad (24)$$

where L_m is a strictly lower triangular matrix whose entries are

$$L_{ij} = \begin{cases} v_i^T v_j, & \text{if } i > j \\ 0 & \text{if } i \leq j \end{cases}. \quad (25)$$

The Neumann series can be used to express the inverse of $(I - A)$ if $\lim_{k \rightarrow \infty} A^k = 0$ (or equivalently, if the spectral radius $\rho(A) < 1$) as [49]

$$(I - A)^{-1} = \sum_{k=0}^{\infty} A^k.$$

The inverse of a general matrix Y can then be found by defining $A = I - Y$

$$(I - A)^{-1} = \sum_{k=0}^{\infty} A^k \quad (26a)$$

$$Y^{-1} = \sum_{k=0}^{\infty} (I - Y)^k. \quad (26b)$$

For the CWY method the inverse of T_m is given by $T_m^{-1} = I + L_m$. Therefore, to find the correction matrix T_m , a Neumann series is used to approximate the inverse of T_m^{-1} (i.e. T_m) using (26b), with $A = (I - T_m^{-1}) = (I - (I + L_m)) = -L_m$.

As an illustrative example, T_3 is shown below for the third iteration ($j = 3$) of the Arnoldi method, where v_4 is orthogonalized against $\{v_1, v_2, v_3\}$

$$T_3 = \begin{bmatrix} 1 & 0 & 0 \\ -\alpha_{21} & 1 & 0 \\ -\alpha_{31} + \alpha_{32}\alpha_{21} & -\alpha_{32} & 1 \end{bmatrix}$$

and $\alpha_{ij} = v_i^T v_j$. In general the values of T_m contain inner products of the columns of matrix V_m and higher order terms containing the product of inner products (i.e. $\alpha_{32}\alpha_{21}$). An approximation of T_m can then be defined through a truncated Neumann series for T_m^{-1} :

$$(I - A)^{-1} = \sum_{k=0}^{\infty} A^k \quad (27a)$$

$$(I - (I - T_m^{-1}))^{-1} = \sum_{k=0}^{\infty} (I - T_m^{-1})^k \quad (27b)$$

$$T_m = \sum_{k=0}^{\infty} (I_m - T_m^{-1})^k = -L_m^k \quad (27c)$$

$$T_m \approx \sum_{k=0}^2 -L_m^k \quad (27d)$$

$$T_m \approx I_m - L_m^1 + L_m^2 \quad (27e)$$

Following (27e) T_3 can then be written as

$$T_3 = \underbrace{\begin{bmatrix} 1 & 0 & 0 \\ -\alpha_{21} & 1 & 0 \\ -\alpha_{31} & -\alpha_{32} & 1 \end{bmatrix}}_{\approx T_3} + \begin{bmatrix} 0 & 0 & 0 \\ 0 & 0 & 0 \\ \alpha_{32}\alpha_{21} & 0 & 0 \end{bmatrix} \quad (28a)$$

$$T_m \approx I - L_m. \quad (28b)$$

If one defines L^0 to be the identity matrix, then the correction matrix T_3 can be expressed with three terms in the series expansion. The full correction matrix T_m can be expressed as the sum of a lower triangular matrix with α_{ij} terms and matrices with the higher-order terms. Truncating the series with two terms will lead to a computationally cheaper approximation of $(V_j^T V_j)^{-1}$ that only includes the inner products $v_i^T v_j$; the local matrix-vector product within the recursion formula (21b) is then avoided.

This method requires one global synchronization per Arnoldi-iteration for the same computation in (23) as the CWY method, and the hybrid version extends naturally. The only difference is the formation of the correction matrix T_j , which now avoids the additional matrix-vector product. The first $(j - 1)$ rows of the first column of (23) will be the j^{th} row of L_{ij} . Once T_j is obtained, the vector v_{j+1} can be orthogonalized by projecting onto the orthogonal complement via (17) with the approximation of the correction matrix T defined in (28b). The norm estimate of v_{j+1} is computed at the end of the j^{th} step, but the true norm is obtained at the following step through computation (23) (row j of column one) after $V_{j:j+1}$ are re-scaled by the norm estimate. The values of the upper Hessenberg matrix $H_{1:j,j}$ are given by the local matrix-vector product $T_j V_j^T v_{j+1}$ from the projection.

The algorithm for H-NCWY follows the outline from Algorithm 4 with Algorithm 6 for computing the correction matrix.

3.2.3 Hybrid Iterated Gauß-Seidel MGS

The correction matrix T_j for CWY and NCWY approximates the interior symmetric matrix $(V_m^T V_m)^{-1}$ with a lower triangular matrix. An alternative version to the WY methods previously presented is to work directly with the formula for the projection matrix and apply a two-step Gauß-Seidel iterative method to the normal equations within. The resulting $T_j^{(2)}$ correction matrix with two-steps will be almost symmetric and a better approximation of $(V^T V)^{-1}$. The method presented here is a

simplified version of the technique originally developed for GMRES by Thomas et al. [53], that requires only one global synchronization.

The projection onto the orthogonal complement at Arnoldi step j is given by

$$Pv_{j+1} = v_{j+1} - V_j x, \quad (29)$$

where the vector x is the solution of the normal equations within the projection onto the orthogonal complement (30a)

$$Pv_{j+1} = v_{j+1} - \underbrace{V_j (V_j^T V_j)^{-1} V_j^T v_{j+1}}_x \quad (30a)$$

$$V_j^T V_j x = V_j^T v_{j+1}. \quad (30b)$$

To solve (30b), a two-step Gauß-Seidel relaxation scheme is used with the matrix splitting $V_j^T V_j = M_j - N_j$, where $M_j = I + L_j$, $N_j = -L_j^T$ and L_j is defined in section 3.2.2. The choice of matrix splitting M_j and N_j was established by Ruhe when it was discovered that MGS employs a multiplicative Gauß-Seidel relaxation scheme [41] (see details in Appendix A of [51]), and further studied in Thomas et. al in [52] with the application to GMRES.

The derivation of the 2-step Gauß-Seidel iteration to the normal equations is as follows:

$$V_j^T V_j x = \underbrace{V_j^T v_{j+1}}_{b_j} \quad (31a)$$

$$(M_j - N_j)x = b_j \quad (31b)$$

$$M_j x^{k+1} = b_j + N_j x^k \quad (31c)$$

$$x^{k+1} = M_j^{-1}(b_j + N_j x^k) \quad (31d)$$

Applying two steps of (31d) with initial guess $x^0 = \mathbf{0}$ yields the following correction matrix T_j :

$$\begin{aligned} x^1 &= M^{-1}b_j \\ x^2 &= M^{-1}(b_j + N_j x^1) \\ x^2 &= \underbrace{M^{-1}[I + NM^{-1}]}_{T_j} b_j \end{aligned}$$

Once the correction matrix T_j is obtained, next vector in the subspace is then projected to the orthogonal complement, similarly to the WY methods, via equation (17).

This method requires one global synchronization, for the same computation $V_{1:j+1}^T V_{j:j+1}$ as in (23), and the hybrid version extends naturally. The first j rows of the second column are the terms $V_j^T v_{j+1}$ that are needed for the projection (17). The j^{th} element of the first column of (23) is the true square norm of the previous vector (obtained after the re-scaling of $V_{j:j+1}$, as in the WY methods). The first $(j-1)$ rows of the first columns are used for the matrices N_j , M_j , and M_j^{-1} ; both M_j and N_j rely on matrix L_j , which are the first $(j-1)$ rows of $V_{1:j+1}^T V_{j:j+1}$ and M_j^{-1} is the correction matrix from CWY in section 3.2.1. The correction matrix T_j is applied in two steps, first the matrix-vector product $a = [I + NM^{-1}]b_j$, followed by a lower triangular solve $Mx = a$. The values for the upper Hessenberg matrix $H_{1:j,j}$ are given by $T_j V_j^T v_{j+1}$. At the end of the orthogonalization, the norm estimate for v_{j+1} is computed using (18), and at the following step, the norm estimate is used to re-scale $V_{j:j+1}$ in order to obtain the true norm from computation (23). The hybrid one-synchronization *Iterated Gauß-Seidel MGS* (H-GSMGS) is outlined in Algorithm 4 with Algorithm 7 for computing the correction matrix.

3.3 Low-synchronization algorithms for the matrix exponential

The low-synchronization methods presented above are based on the same principles in terms of the reformulation of the orthogonalization process paired with a lagged normalization to group inner products in a way that reduces the global communication to one per Arnoldi step. We extend the low-synchronization methods to include a norm estimate in order to avoid multiplying matrix A with a vector v_j with a large norm. We then compute the true norm and normalize at the subsequent step (referred to as hybrid). The key difference between each algorithm presented is the choice of the approximation to the interior symmetric matrix $(V^T V)^{-1}$. An outline of a hybrid low-synchronization method is presented in Algorithm 4 where the details are provided for the global communication, and additional scaling and computation needed for the hybrid algorithms. At line 24, this algorithm can be paired with Algorithms 5, 6, or 7 for computing a correction matrix T and obtaining the values for the upper Hessenberg matrix H_m .

Once the components V_m and H_m of the Krylov subspace are obtained from Algorithm 4, the matrix-exponential times a vector can be computed using the Krylov projection formula (13). If A (line 12 of Algorithm 4) is the augmented matrix from section 2.1 then one matrix function evaluation is needed within an exponential integrator to obtain all φ -functions.

Algorithm 4 Hybrid low-synchronization Arnoldi

```
1: procedure HGSMGS( $m, b$ )                                     ▷ size of subspace, initial vector
2:   if H-CWY or H-NCWY then
3:      $T_{1:m,1:m} = I_m$                                        ▷ initialize correction matrix to identity
4:   else                                                       ▷ if using H-GSMGS
5:      $M_{1:m,1:m} = I_m$                                        ▷ initialize to identity matrix
6:      $M_{1:m,1:m}^{-1} = I_m$                                        ▷ initialize to identity matrix
7:      $N_{1:m,1:m} = 0_m$                                        ▷ initialize to zero matrix
8:    $v_1 = b$ 
9:    $j = 0$ 
10:  while  $j < m$  do
11:     $j = j+1$ 
12:     $v_{j+1} = Av_j$                                              ▷ next vector in basis
13:     $\mathbf{temp} = V_{1:j+1}^T V_{j:j+1}$                                ▷ MPI_AllReduce; computation (23)
14:    if  $j > 1$  then
15:       $V_{j:j+1} = V_{j:j+1} * \mathbf{nrm\_est}$                        ▷ re-scale by previous norm estimate
16:       $\mathbf{true\_nrm} = \sqrt{\mathbf{temp}_{j,1}}$                          ▷ true norm of prev. vector
17:      if  $j == 1$  then
18:         $\beta = \mathbf{true\_nrm}$                                    ▷ norm of initial vector
19:         $V_{j:j+1} = V_{j:j+1} / \mathbf{true\_nrm}$                        ▷ scale for Arnoldi
20:         $\mathbf{temp}_{:,2} = \mathbf{temp}_{:,2} / \mathbf{true\_nrm}$            ▷ scale for Arnoldi
21:         $\mathbf{temp}_{j:j+1,2} = \mathbf{temp}_{j:j+1,2} / \mathbf{true\_nrm}$ 
22:      if  $j > 1$  then                                           ▷ form projection matrices
23:         $\mathbf{temp}_{1:j-1,1} / = \mathbf{true\_nrm}$                        ▷ scale for Arnoldi
24:         $H_{i,j,j} = \mathbf{form\_T}$                                    ▷ see algo. 5, 6, 7
25:         $H_{j-1,j} = \mathbf{true\_nrm}$                                ▷ set previous norm
26:         $v_{j+1} = v_{j+1} - V_j H_{1:j,j}$                              ▷ orthogonalize
27:         $ss = \sum \mathbf{temp}_{1:j,2}^2$ 
28:        if  $\mathbf{temp}_{j+1,2} < ss$  then
29:           $\mathbf{nrm} = \text{MPI.AllReduce}$ 
30:        else
31:           $\mathbf{nrm\_est} = \sqrt{\mathbf{temp}_{j+1,2} - ss}$                ▷ norm estimate from [23]
32:          if  $\mathbf{nrm\_est} \approx 0$  then                             ▷ check for lucky breakdown [32]
33:             $\mathbf{happy\_breakdown} = \text{True}$ 
34:            break
35:           $v_{j+1} = v_{j+1} / \mathbf{nrm\_est}$                          ▷ “normalize”
36:         $\mathbf{nrm} = \sqrt{v_{m+1}^T v_{m+1}}$                                ▷ MPI_AllReduce norm of last vector
37:         $V_{m+1} = V_{m+1} / \mathbf{nrm}$ 
38:         $H_{m+1,m} = \mathbf{nrm}$ 
```

Algorithm 5 Hybrid CWY Correction Matrix (sect. 3.2.1)

- 1: **procedure** HCWY_T(\mathbf{temp}, T) ▷ inner products (line 13 algo. (4)), correction matrix
 - 2: $T_{j,1:j-1} = -\mathbf{temp}_{1:j-1,1}^T T_{1:j-1,1:j-1}$ ▷ Correction matrix via (21b)
 - 3: $H_{1:j,j} = T_j \mathbf{temp}_{1:j,2}$ ▷ Hessenberg values
-

Algorithm 6 Hybrid NCWY Correction Matrix (sect. 3.2.2)

- 1: **procedure** HNCWY_T(\mathbf{temp}) ▷ inner products (line 13 algo. (4))
 - 2: $T_{j,1:j-1} = -\mathbf{temp}_{1:j-1,1}^T$ ▷ Correction matrix (28b)
 - 3: $H_{1:j,j} = T_j \mathbf{temp}_{1:j,2}$ ▷ Hessenberg values
-

Algorithm 7 Hybrid Iterated Gauß-Seidel Correction Matrix (sect. 3.2.3)

- 1: **procedure** HGSMGS_T(\mathbf{temp}) ▷ inner products (line 13 algo. (4))
 - 2: $M_{j,1:j-1} = \mathbf{temp}_{1:j-1,1}^T$
 - 3: $N_{1:j-1,j} = -\mathbf{temp}_{1:j-1,1}$
 - 4: $M_{j,1:j-1}^{-1} = -\mathbf{temp}_{1:j-1,1}^T M_{1:j-1,1:j-1}^{-1}$
 - 5: $p = [I_j + N_{1:j,1:j} M_{1:j,1:j}^{-1}] \mathbf{temp}_{1:j,2}$ ▷ Part 1: mat-vec
 - 6: $H_{1:j,j} = \mathbf{triang_sol}(M_{1:j,1:j}, p)$ ▷ Part 2: lower triangular solve + Hessenberg values
-

4 Numerical Experiments

4.1 Application to exponential time integration

Over the past several decades significant amount of research on exponential integrators resulted in development of many classes of efficient and accurate methods of this type. Initially exponential methods were used to solve diffusion or diffusion-reaction systems [18, 20] but with time the range of applications of these techniques increased. Exponential integrators were used in computational weather prediction [7, 21, 38], combustion [50], astrophysics [15, 16, 17], and other applications where the methods were shown to be competitive with state-of-the-art techniques for solving stiff PDEs. Exponential integrators of various types have been developed such as multistep [21], Runge-Kutta [33, 11, 34, 55], Rosenbrock [12, 26, 15, 16], polynomial [5], exponential parareal [6, 14, 27] and more.

The motivation for extending the low-synchronization methods to exponential integrators is to improve the integrator's parallel performance and strong scaling properties for solving large-scale stiff PDEs. Our primary application of interest is the shallow-water (SW) equations, but three additional examples are presented as a proof-of-concept to illustrate the benefits of the low-synchronization methods. Given that our primary application relates to weather prediction, we use exponential integrators that were developed and tested for the SW equations. The exponential multistep methods were presented in [21] and were shown to produce accurate, physically plausible results even with large timesteps [21]. In addition, we also study performance of the newly developed stiffly-resilient exponential Runge-Kutta type integrators (SRERK) which are constructed to mitigate issues with order reduction when solving stiff differential equations [11]. The new SRERK methods have not been studied as extensively as other exponential methods and the stiff SW equations are a good test problem for these techniques. The set of the time integrators of different order we chose

is diverse enough for a thorough study of the low-synchronization methods and their effect on the parallel efficiency of exponential methods for our application. The multistep and Ruge-Kutta type integrators that are used for our experiments are listed below.

- 4th, 5th, and 6th order exponential multi-step methods (epi) [21]

$$u_{n+1} = u_n + \varphi_1(hJ_n)hf_n + \sum_{m=1}^M \varphi_m(hJ_n)v_m \quad (32a)$$

$$v_m = \sum_{i=1}^P \alpha_{m,i}hR(u_{n-i}) \quad (32b)$$

$$R(u_{n-i}) = f_{n-i} - f_n - J_n(u_{n-i} - u_n) \quad (32c)$$

with coefficients $\alpha_{m,i}$

$$A_4 = \begin{pmatrix} 0 & 0 \\ \frac{-3}{10} & \frac{3}{40} \\ \frac{32}{5} & \frac{-11}{10} \end{pmatrix}$$

$$A_5 = \begin{pmatrix} 0 & 0 & 0 \\ -\frac{4}{5} & \frac{2}{5} & -\frac{4}{45} \\ 12 & -\frac{9}{2} & \frac{8}{9} \\ 3 & 0 & -\frac{1}{3} \end{pmatrix}$$

$$A_6 = \begin{pmatrix} 0 & 0 & 0 & 0 \\ -\frac{49}{60} & \frac{351}{560} & -\frac{359}{12600} & \frac{367}{6720} \\ \frac{97}{7} & -\frac{14}{99} & \frac{63}{176} & -\frac{1}{2} \\ \frac{485}{21} & -\frac{151}{14} & \frac{23}{9} & -\frac{31}{168} \end{pmatrix}$$

- 3rd order Stiffly Resilient Exponential Runge-Kutta (SRERK3) [11]

$$z_1 = u_n + \varphi_1\left(\frac{3}{4}hJ_n\right)\frac{3}{4}hf(u_n) \quad (33a)$$

$$u_{n+1} = u_n + \varphi_1(hJ_n)hf(u_n) + \varphi_3(hJ_n)\frac{32}{9}hR(z_1) \quad (33b)$$

- 6th order SRERK6 [11]

$$z_i = u_n + \varphi_1(c_i hJ_n)c_i hf(u_n) \quad i \in \{1, 2\} \quad (34a)$$

$$z_j = u_n + \varphi_1(c_j hJ_n)c_j hf(u_n) + \varphi_3(c_j hJ_n)c_j^3 \sum_{k=1}^2 \beta_{3,k}hR(z_k) \quad (34b)$$

$$+ \varphi_4(c_j hJ_n)c_j^4 \sum_{k=1}^2 \beta_{4,k}hR(w_k) \quad j \in \{3, 4, 5, 6\} \quad (34c)$$

$$u_{n+1} = u_n \varphi_1(hJ_n)hf(u_n) + \varphi_3(hJ_n) \sum_{k=3}^6 \alpha_{3,k}hR(z_k) + \varphi_4(hJ_n) \sum_{k=3}^6 \alpha_{4,k}hR(z_k) \quad (34d)$$

$$+ \varphi_5(hJ_n) \sum_{k=3}^6 \alpha_{5,k}hR(z_k) + \varphi_6(hJ_n) \sum_{k=3}^6 \alpha_{6,k}hR(z_k) \quad (34e)$$

with $c = [\frac{10-\sqrt{10}}{15}, \frac{10+\sqrt{10}}{15}, \frac{1}{4}, \frac{1}{2}, \frac{2}{4}, 1,]$,

$$\beta_{i,k} = \begin{bmatrix} \frac{155+65\sqrt{10}}{18} & \frac{155-65\sqrt{10}}{18} \\ \frac{-100-55\sqrt{10}}{4} & \frac{-100-55\sqrt{10}}{4} \end{bmatrix} \quad \alpha_{j,k} = \begin{bmatrix} 128 & -48 & \frac{128}{9} & -2 \\ -1664 & 912 & -\frac{896}{3} & 44 \\ 9216 & -6144 & \frac{7168}{3} & -384 \\ -20480 & 15360 & -\frac{20480}{3} & 1280 \end{bmatrix}$$

Both the multistep and Runge-Kutta -type integrators require the computation of a linear combination of the exponential-like φ -functions times a vector (sec. 2.1). To compute linear combinations (4), our algorithm of choice is KIOPS (outlined in Algorithm 8, referenced in 2.3.1) [22]. The integrators are implemented in order to minimize the number of KIOPS calls per timestep. Each multistep method will require one call to KIOPS to compute the linear combination of φ -functions in order to advance the solution to the next timestep t_{n+1} (e.g. equation (32a)). SRERK3 will require two calls to KIOPS, one for the stage and one to advance the solution. Finally, SRERK6 will require six calls to KIOPS, one to advance the solution (eg. (34d) - (34e)), one for the stages z_i , and four calls to stage z_j (e.g. (34b) - (34c)).

To compare the performance of the low-synchronization GS variants, we implement the orthogonalization methods discussed in sections 3.2.1 to 3.2.3 within the KIOPS algorithm. A parallel implementation based on an incomplete-orthogonalization Classical Gram-Schmidt (ioCGS) is provided in the supplementary material of [21]. KIOPS is adapted in line 3 of Algorithm 8 to compare the efficiency of exponential integrators with the full-orthogonalization, low-synchronization, MGS variants against the reference ioCGS algorithm. The adaptivity for τ_i and m_i remains the same throughout the experiments, allowing for a fair comparison between the orthogonalization techniques.

Algorithm 8 Krylov Incomplete Orthogonalization Process (KIOPS) [22]

- 1: **procedure** KIOPS(A, b, m, τ_{final}) ▷ matrix, initial vector, size of subspace, final τ
 - 2: **while** substepping in τ **do**
 - 3: Compute Arnoldi Decomposition: **Arnoldi**(A, b, m) (eg. alg. (1))
 - 4: Compute matrix exponential using (13)
 - 5: Compute local error estimate for step τ_i (eqn. (36) in [22])
 - 6: Compute suggested new parameters τ_{new} and m_{new} (eqn. (44) and (46) in [22])
 - 7: Decide to accept or reject solution at step τ_i (sect. 3.5 in [22])
-

4.2 Experimental set-up

We highlight the strong-scaling parallel efficiency of the five exponential integrators with each of the hybrid low-synchronization methods presented in sections 3.2.1 to 3.2.3. To complement the strong scaling² plots, the runtime ratio between the reference algorithm ioCGS and each of the hybrid low-synchronization methods is presented in a table. The runtime ratio for a low-synchronization method ls is computed as

$$\text{runtime_ratio}_{ls} = \text{runtime}_{ls} / \text{runtime}_{ioCGS}$$

²Strong scaling refers to the application’s performance or runtime when the problem size is fixed and the number of processors varies.

where a runtime ratio below 1.0 implies that the exponential integrator with the low-synchronization method is more efficient than a version with an incomplete Classical Gram-Schmidt orthogonalization scheme. To avoid pollution of the data from the machine state variability, 5 runs are performed and the median is reported in strong scaling plots for each problem and integrator.

Performance studies were conducted on the Lenovo ThinkSystem supercomputer of Shared Services Canada. This cluster runs Linux on Intel® Xeon® Platinum 8380 CPU 2.30GHz processors, equipped with 512 GB of memory per node, and utilizes an Infiniband HDR network.

4.3 Moderate Scale Example PDEs

For the proof-of-concept tests of the performance of the low-synchronization methods compared to standard Krylov algorithms, we choose problems that are routinely used to study the performance of stiff integrators:

- Allen-Cahn (AC) equation [3]

$$\frac{\partial u}{\partial t} = \epsilon \nabla^2 u + u - u^3 \quad (35)$$

with no-flow boundary conditions on $x, y \in [-1, 1]$ and a diffusion coefficient of $\epsilon = 0.1$. The initial condition is given by

$$u(x, y, t = 0) = 0.1 + 0.1 \cos(2\pi x) \cos(2\pi y) \quad (36)$$

with a final time of integration to be $t_f = 0.02$ and a timestep of $dt = 10^{-2}$.

- Advection-Diffusion-Reaction (ADR) [10]

$$\frac{\partial u}{\partial t} = \epsilon \nabla^2 u - \alpha(u_x + u_y) + \gamma u(u - \frac{1}{2})(1 - u) \quad (37)$$

where homogeneous Neumann boundary conditions are imposed on $x, y \in [0, 1]$. The coefficients ϵ and α measure the diffusion and advection respectively. For this scenario, we consider an advection-dominated regime with $\epsilon = 10^{-2}$ and $\alpha = -6$, with the initial condition given by

$$u(x, y, t = 0) = 0.3 + 256(xy(1-x)(1-y))^2. \quad (38)$$

We chose the final time of integration to be $t_f = 10^{-1}$ with a timestep of $dt = 10^{-2}$

- Burger's equation (BURG)

$$\frac{\partial u}{\partial t} = -\frac{1}{2} \left(\frac{\partial u^2}{\partial x} + \frac{\partial u^2}{\partial y} \right) + \epsilon \nabla^2 u \quad (39)$$

with Dirichlet boundary conditions on $x, y \in [0, 1]$. The initial condition is given by

$$u(x, y, t = 0) = \sin(3\pi x)^2 \sin(3\pi y)^2 (1 - y). \quad (40)$$

We choose a final time of $t_f = 0.04$ with a timestep of $dt = 10^{-2}$, and $\epsilon = 10^{-3}$.

In all problems, the number of degrees of freedom is $N = 2000^2$, and second order finite differences are used to approximate the first and second spatial derivatives. Strong scaling results with processor sizes $p = [100, 400, 625, 1600, 2500]$ are presented, and a Krylov tolerance of 10^{-12} is used within KIOPS.

4.3.1 Strong Scaling Results

The strong scaling results for AC are shown in Figures 1 - 3, for ADR in 4 - 6, and BURG in Figures 7 - 9, with the tables for runtime ratios displayed in Tables 1, 2, and 3 respectively.

Overall, the degree of improvement varied for each example problem, however, it is clear that the low-synchronization methods perform on-par if not better than the reference incomplete CGS algorithm. Our numerical experiments show that the greater computational complexity of the low-synchronization algorithms does not significantly slow down the runtime for these moderately sized example problems. The AC example displays the largest amount of runtime savings for all integrators. Meanwhile, the runtime for Burger’s equation with the low-synchronization algorithms remains nearly identical to the reference `ioCGS`. This is in-line with our performance expectations for these moderately sized problems on a relatively small number of processors, given that the low-synchronization methods were designed for massively parallel systems and large scale problems. It is informative to see that there is no penalty for using these methods on a purely distributed memory framework; we are not using GPUs. Now we discuss the results of each individual problem in greater detail.

For AC, both the `epi` and `srerk` integrators showed significant improvement with all three low-synchronization methods (see Figures 1 - 3). The greatest improvement for an `epi` integrator is seen for `epi6` with a 40% reduction in runtime with `H-NCWY` with 2500 processors (see Table 1). For the `srerk` integrators (Figure 3), the greatest improvement is seen for `srerk6` with a 31% reduction in runtime with `H-CWY` with 1600 and 2500 processors. This test problem is a clear example of the improved performance of exponential integrators with a low-synchronization Arnoldi method.

For ADR, there are improvements with the `epi` integrators (see Figure 4 - 5) and marginal to no improvement with the `srerk` integrators (see Figure 6). The greatest improvement for an `epi` integrator is seen for `epi5` with a 25% reduction in runtime with `H-NCWY` with 1600 processors (see Table 2). For the `srerk` integrators, there were marginal improvements with `srerk3`, at most 15% reduction in runtime with `H-NCWY` for 2500 processors (see Figure 6 and Table 2). Meanwhile, the results for `srerk6` displayed little to no improvement. For processor sizes less than 2500, all methods were slightly slower compared to `ioCGS` and showed marginal improvement for for 2500 processors.

For Burger’s equation, both `epi` and `srerk` integrators performed similarly between the low-synchronization method and `ioCGS`. The most significant improvement over all integrators is shown for `epi4` with 2500 processors with a 25% reduction in runtime with `H-NCWY`. For the `srerk` integrators, the strong scaling curves display nearly overlapping lines, indicating the runtime of the low-synchronization methods are on-par with the reference `ioCGS`. Small improvements ($\leq 9\%$) are seen for both `srerk` integrators with `H-NCWY` and `H-CWY` for processors larger than 100.

For this tests set, it remains unclear which low-synchronization methods is more favorable. In the AC and ADR `epi` strong scaling results (Figures 1 - 2 and 4 - 5) (where the three low-synchronization methods showed to be more efficient) the runtime between the three low-synchronization methods is nearly identical, as shown by the strong scaling curves are nearly overlapping. However, for the largest processor size the best results are achieved with either `H-CWY` or `H-NCWY`, (see Tables 1 and 2).

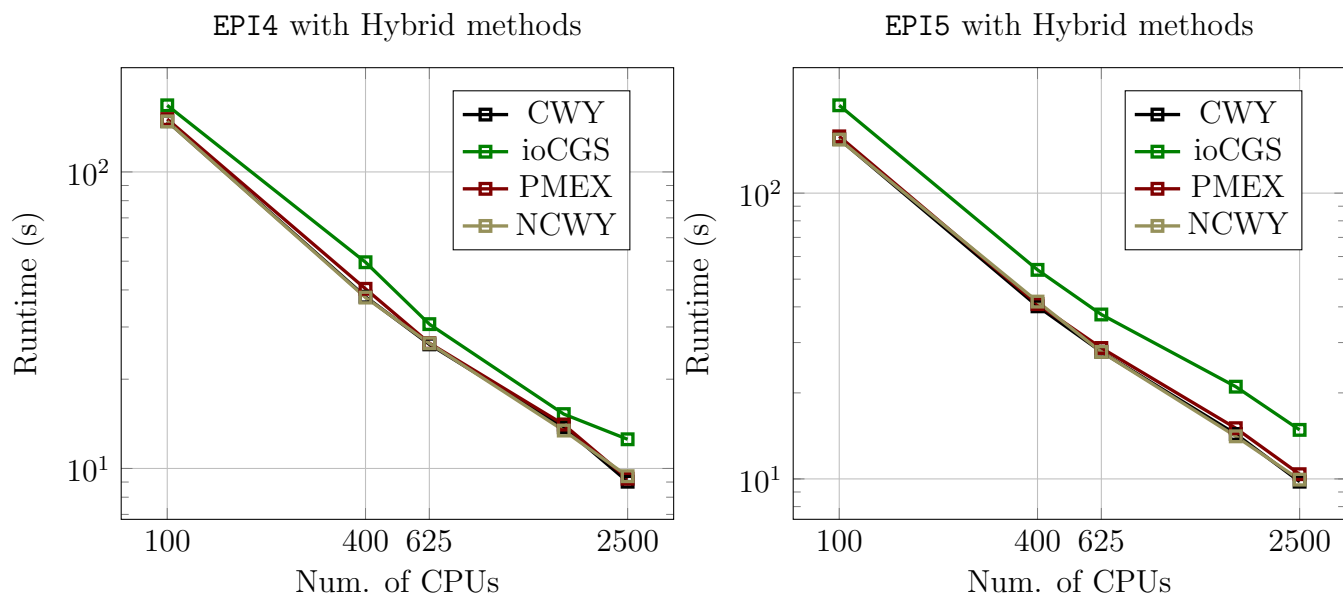


Figure 1: Strong scaling results for AC with low-synchronization hybrid methods for epi4 and epi5.

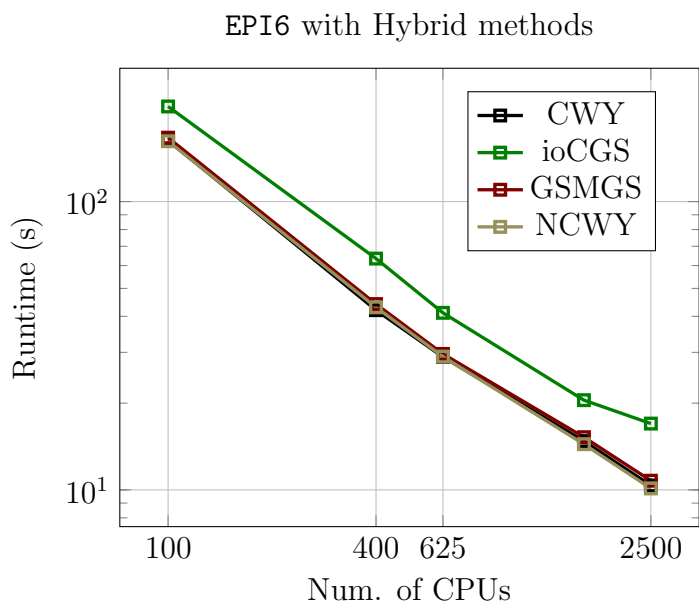


Figure 2: Strong scaling results for AC with low-synchronization hybrid methods for epi6.

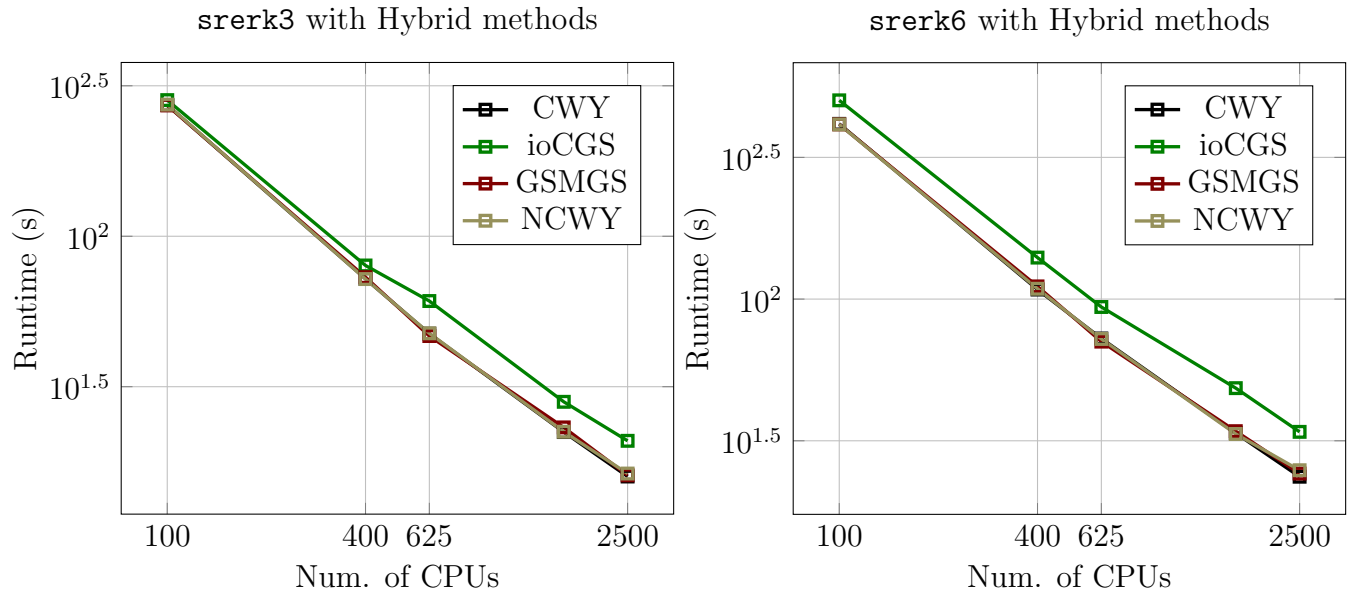


Figure 3: Strong scaling results for AC with low-synchronization hybrid methods for `srrerk` integrators.

low-synchronization Method	p	EPI4	EPI5	EPI6	SRERK3	SRERK6
H-GSMGS	100	0.90	0.78	0.78	0.96	0.82
	400	0.81	0.76	0.70	0.91	0.79
	625	0.86	0.76	0.72	0.77	0.75
	1600	0.92	0.72	0.74	0.82	0.71
	2500	0.74	0.70	0.63	0.77	0.71
H-NCWY	100	0.88	0.76	0.76	0.97	0.82
	400	0.76	0.77	0.68	0.90	0.78
	625	0.86	0.74	0.70	0.78	0.77
	1600	0.88	0.67	0.70	0.80	0.69
	2500	0.75	0.67	0.60	0.78	0.73
H-CWY	100	0.88	0.76	0.76	0.96	0.83
	400	0.77	0.75	0.66	0.90	0.77
	625	0.85	0.74	0.70	0.78	0.77
	1600	0.90	0.68	0.72	0.79	0.69
	2500	0.72	0.66	0.61	0.76	0.69

Table 1: Runtime ratios of low-synchronization/ioCGS for Allen-Cahn pde.

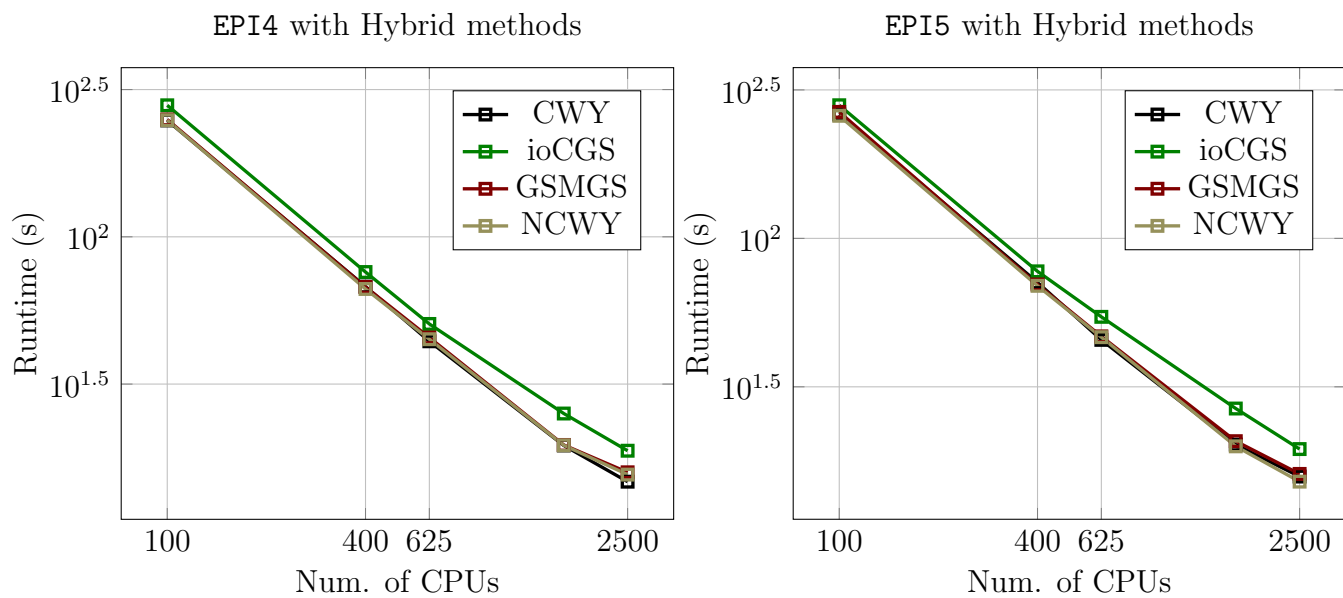


Figure 4: Strong scaling results for ADR with low-synchronization hybrid methods for epi4 and epi5.

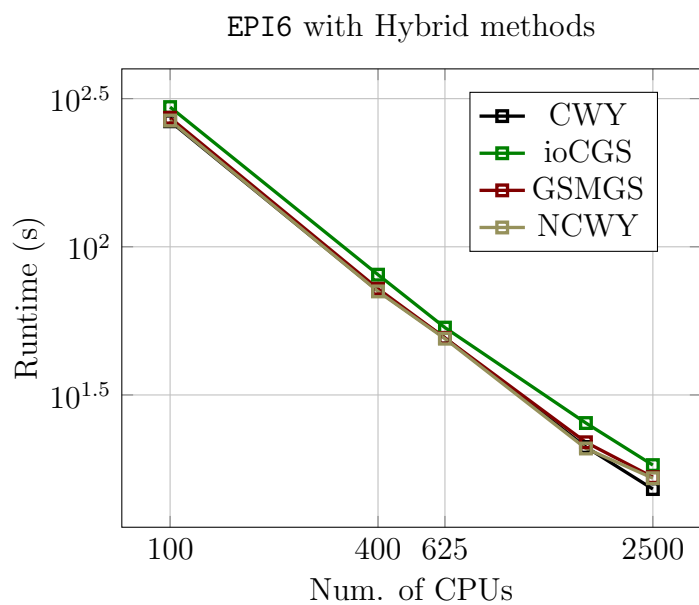


Figure 5: Strong scaling results for ADR with low-synchronization hybrid methods for epi6.

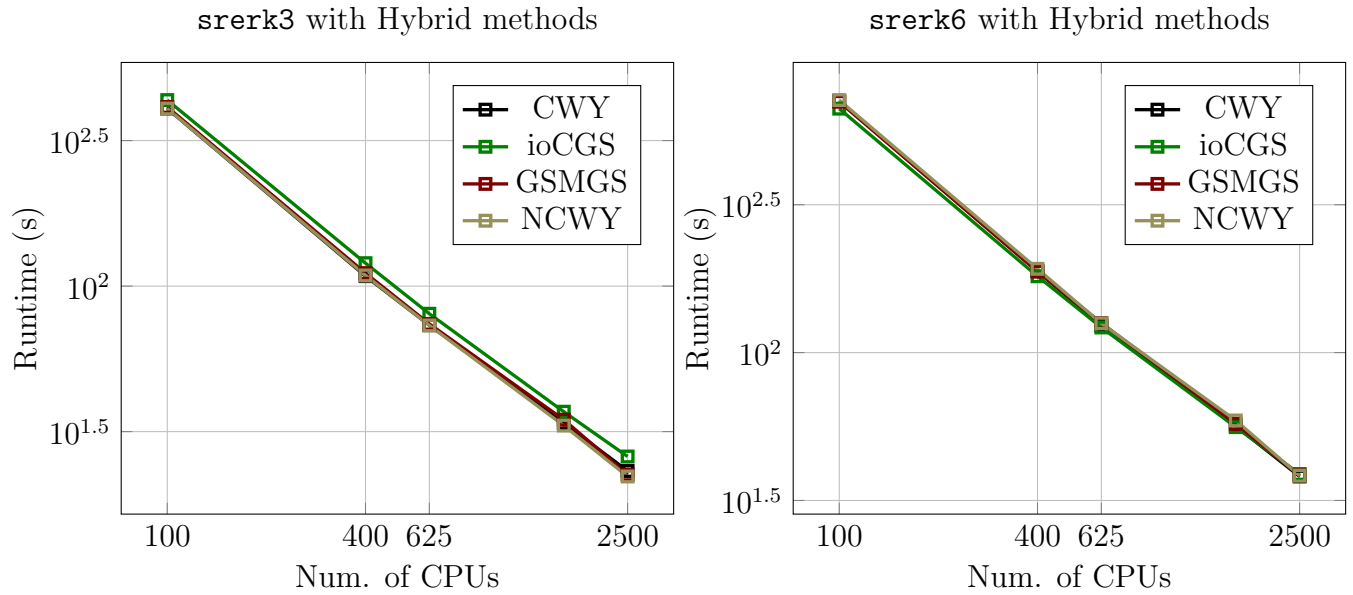


Figure 6: Strong scaling results for ADR with low-synchronization hybrid methods for `srrerk3` and `srrerk6`.

low-synchronization Method	p	EPI4	EPI5	EPI6	SRERK3	SRERK6
H-GSMGS	100	0.90	0.95	0.92	0.95	1.06
	400	0.89	0.90	0.90	0.92	1.04
	625	0.90	0.86	0.92	0.92	1.03
	1600	0.78	0.78	0.86	0.94	1.03
	2500	0.84	0.82	0.91	0.87	0.99
H-NCWY	100	0.89	0.92	0.90	0.94	1.07
	400	0.88	0.89	0.88	0.91	1.06
	625	0.89	0.85	0.92	0.91	1.03
	1600	0.78	0.75	0.82	0.90	1.05
	2500	0.83	0.78	0.90	0.85	0.99
H-CWY	100	0.89	0.93	0.90	0.94	1.06
	400	0.89	0.92	0.88	0.90	1.04
	625	0.87	0.84	0.92	0.91	1.08
	1600	0.78	0.76	0.83	0.91	1.0
	2500	0.78	0.81	0.83	0.89	0.99

Table 2: Runtime ratios of low-synchronization/ioCGS for Advection-Diffusion-Reaction.

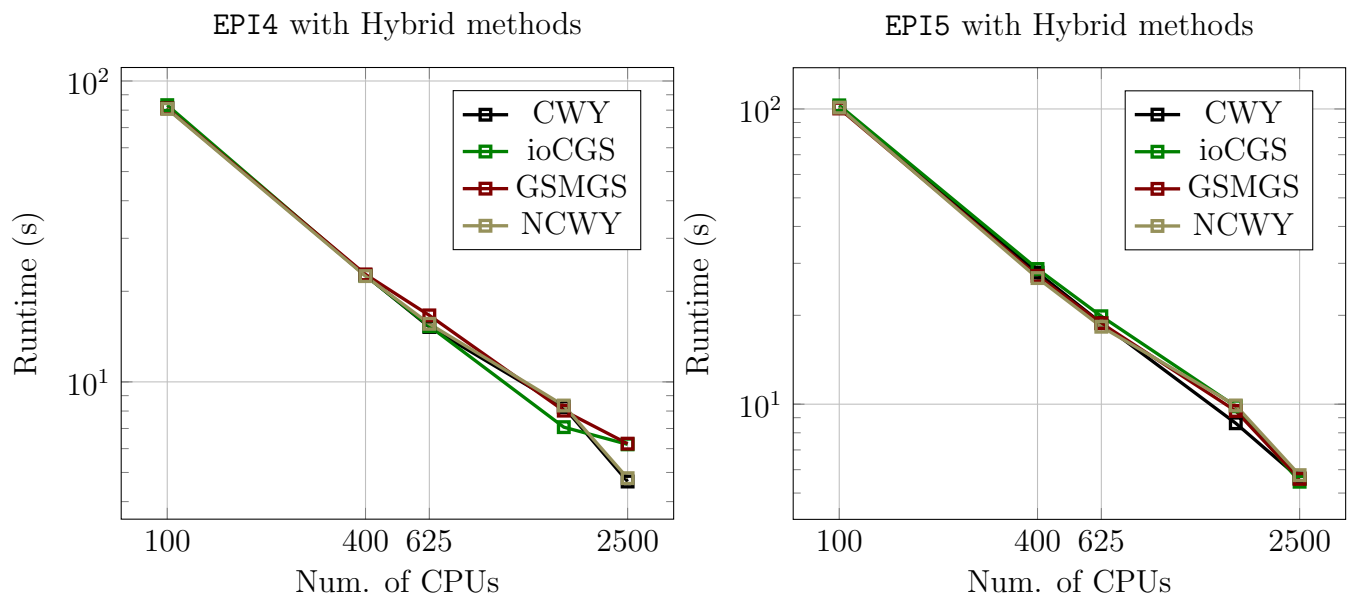


Figure 7: Strong scaling results for Burger's with low-synchronization hybrid methods for epi4 and epi5.

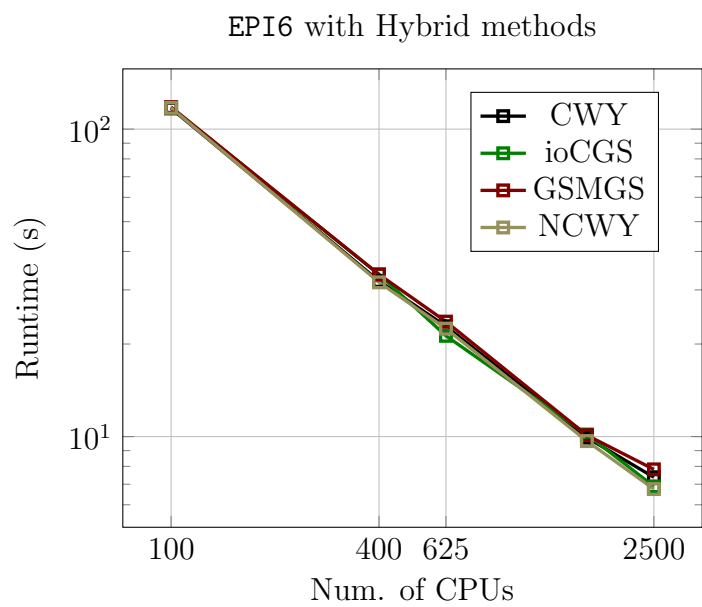


Figure 8: Strong scaling results for Burger's with low-synchronization hybrid methods for epi6.

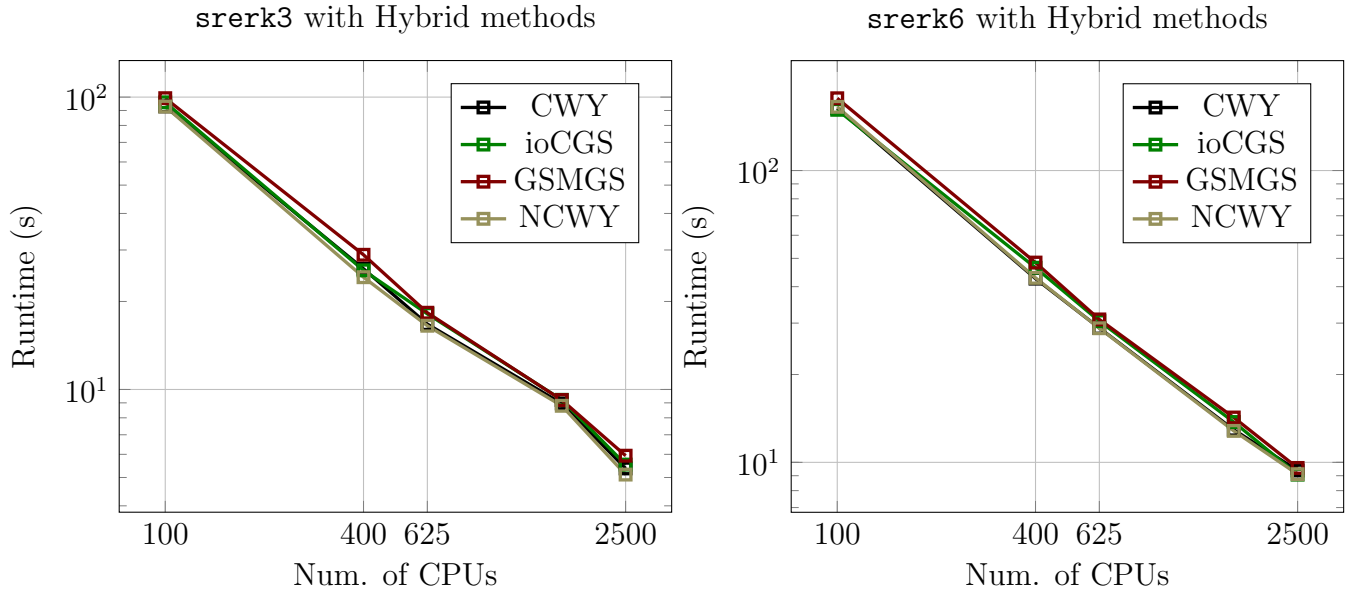


Figure 9: Strong scaling results for Burger's with low-synchronization hybrid methods for srrerk integrators.

low-synchronization Method	p	EPI4	EPI5	EPI6	SRERK3	SRERK6
H-GSMGS	100	0.98	0.98	1.00	1.03	1.10
	400	1.01	0.95	1.00	1.13	1.04
	625	1.09	0.95	1.11	1.01	1.01
	1600	1.13	0.96	0.99	1.00	1.04
	2500	1.01	1.02	1.14	1.07	1.05
H-NCWY	100	0.97	0.98	1.00	0.97	1.02
	400	1.00	0.93	0.94	0.95	0.92
	625	1.02	0.92	1.06	0.91	0.95
	1600	1.18	1.01	0.95	0.95	0.93
	2500	0.77	1.05	0.98	0.92	1.00
H-CWY	100	0.98	0.99	0.99	0.97	1.01
	400	1.00	0.97	0.95	1.01	0.92
	625	0.99	0.95	1.07	0.92	0.95
	1600	1.17	0.88	0.98	0.97	0.94
	2500	0.75	1.03	1.07	0.97	1.03

Table 3: Runtime ratios of low-synchronization/ioCGS for inviscid Burger's pde.

4.4 Large Scale Shallow-Water Equations

We now present the results for the shallow water (SW) equations on the cubed-sphere, as presented in [21]. The SW equations are frequently used as a benchmark for assessing numerical methods in geophysical fluid dynamics and serve as a simplified model of choice for numerical weather prediction [58].

We solve the SW equations using a direct flux reconstruction (DFR) spatial discretization [21, 28, 40]. The computational grid is made up of $6 \times N_e \times N_e$ elements, each element with $N_s \times N_s$ solution points. We use $N_e = 168$ elements with $N_s = 7$ grid points, for a total of approximately 8.2 million degrees of freedom (8,297,856 total grid points). All simulations are carried out with a timestep of 900 seconds, a Krylov tolerance within KIOPS of 10^{-12} , and a final time of 4 hours. The strong scaling results are carried out for processor sizes of $p = [864, 1176, 2646, 4704, 10584]^3$ on the following standard benchmark cases:

- **SW-C5:** Zonal flow over isolated mountain (case 5 from Williamson et. al. [58])
- **SW-C6:** Rossby-Haurwitz wavenumber-4 (case 6 from Williamson et. al. [58])
- **SW-C8:** Unstable jet-stream from Galewsky et. al. [19]

4.4.1 Strong Scaling Results

The strong scaling results for SW-C5 are shown in Figures 10 - 12, SW-C6 is shown in 13 - 15, and SW-C8 is shown in 16 - 18 with the corresponding Tables 4, 5, 6 for SW-C5, SW-C6, and SW-C8 respectively.

For these larger scale problems, we see the low-synchronization methods outperformed `ioCGS` for all cases when the number of processors was large enough. This is precisely what is expected given that for large number of processors the savings in communication that the low-synchronization methods offer play the key role in the overall time-to-solution of the exponential methods. The numerical test results support our hypothesis and highlight the advantages of the low-synchronization methods for very large scale stiff problems that have to be solved on massively parallel computing platforms. For this example set, the `H-GSMGS` algorithm showed the most improvement in performance. This could be explained by `H-GSMGS` having the largest computational complexity for computing the correction matrix T (matrix-matrix product of M^{-1} and N , and a lower triangular solve), as it is advantageous to increase the computational intensity in a parallel setting [35].

Of the three geophysical scenarios presented, exponential integrators for the Rossby-Haurwitz waves test problem (SW-C6) showed the most improvement in time-to-solution and scaling properties; see Figures 13 - 15 and Table 5. First, all integrators showed an improved performance with the low-synchronization methods compared to `ioCGS` starting from the smallest processor size of 864 CPUs. The greatest improvement over all integrators is a 45% reduction in runtime for `epi6` with `H-GSMGS` for $10k$ processors. The integrators were consistently faster with `H-GSMGS` compared to `H-CWY` and `H-NCWY`, where the `H-WY` methods slowed down for $1k$ processors. Second, the integrators displayed better strong scaling properties with the low-synchronization methods. The `epi` methods display zig-zaggy behavior with `ioCGS` and show little improvement in runtime between $4k$ and $10k$ processors, while the strong scaling curves with the low-synchronization methods remains fairly linear.

The results for zonal flow over mountain (SW-C5) showed smaller gains but improvements were still observed once the number of processors exceeded $4k$; see Figures 10 - 12 and Table 4. Exponential integrators with `ioCGS` remained more efficient for up to $4k$ processors for both `epi` and `srerk` type. For the `epi` integrators, the greatest improvement was seen with `epi5` with a 15% reduction in runtime with `H-NCWY` and `H-CWY`. For the `srerk` integrators, the `srerk3` saw the best improvement with a 16% reduction in runtime with `H-GSMGS`.

³For brevity, when referencing a specific processor size, the short hand k (short for kilo which denotes 1000) will be used for size, i.e. $2k$ instead of 2646

The unstable jet stream (SW-C8) case presented intermediate improvements with the low-synchronization methods with all exponential integrators; see Figures 16 - 18 and Table 6. The strong scaling graphs for the `epi` methods show a similar runtime between `ioCGS` and `H-GSMGS` for processors fewer than $2k$, followed by an improvement in performance by `H-GSMGS` as the number of processors increased (see Figures 16 - 17). Performance with the `H-WY` methods improved for more than $4k$ processors with `epi4` and the `srerk` type, and more than $2k$ for `epi5` and `epi6`. The largest improvement was for `epi6` with a 30% reduction in runtime using `H-GSMGS` with $10k$ processors.

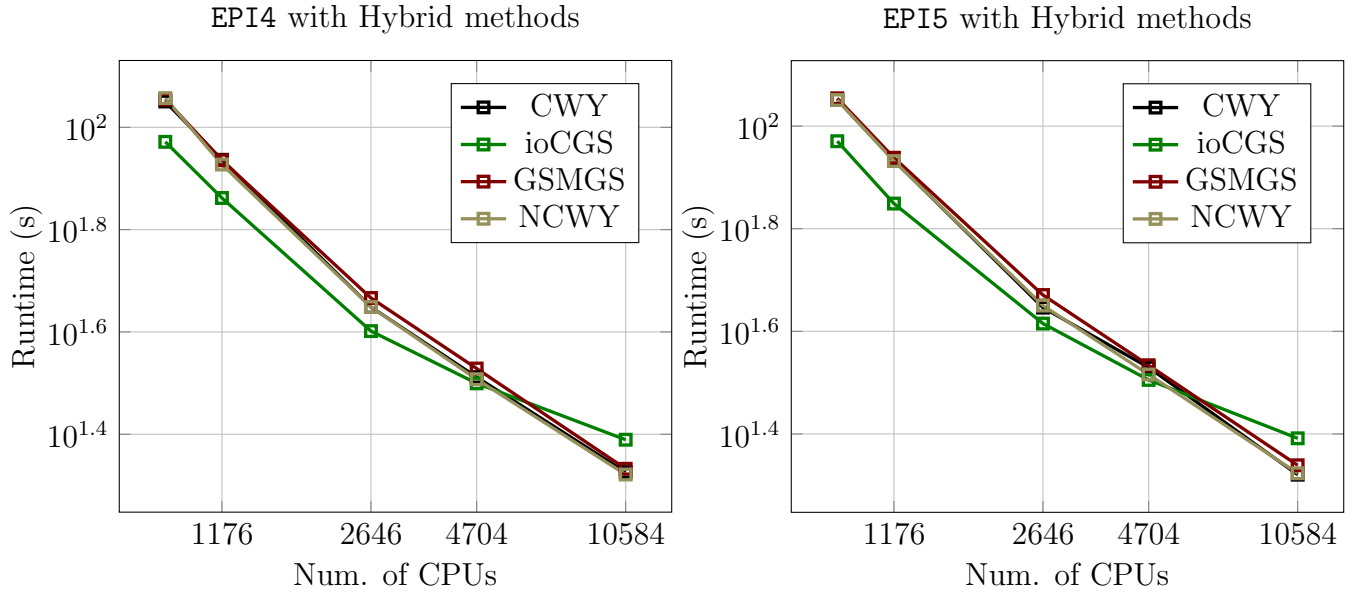


Figure 10: Strong scaling results for `epi4` and `epi5` with hybrid low-synchronization methods for SW-C5.

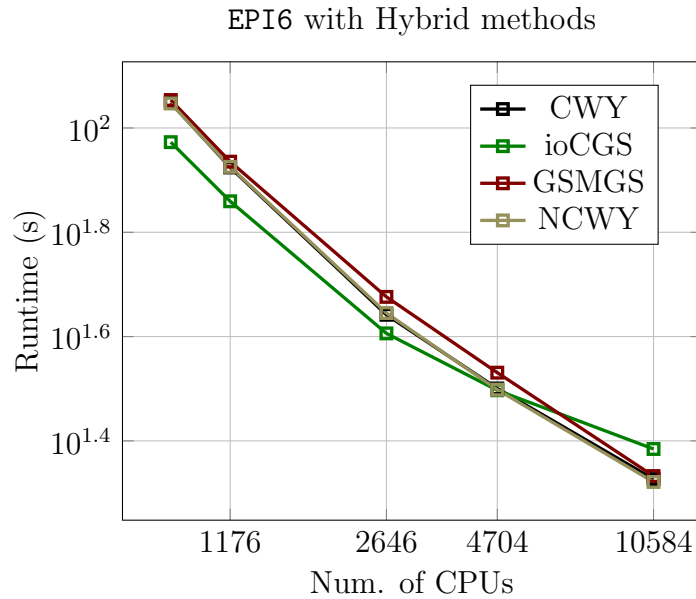


Figure 11: Strong scaling results for `epi6` with hybrid low-synchronization methods for SW-C5.

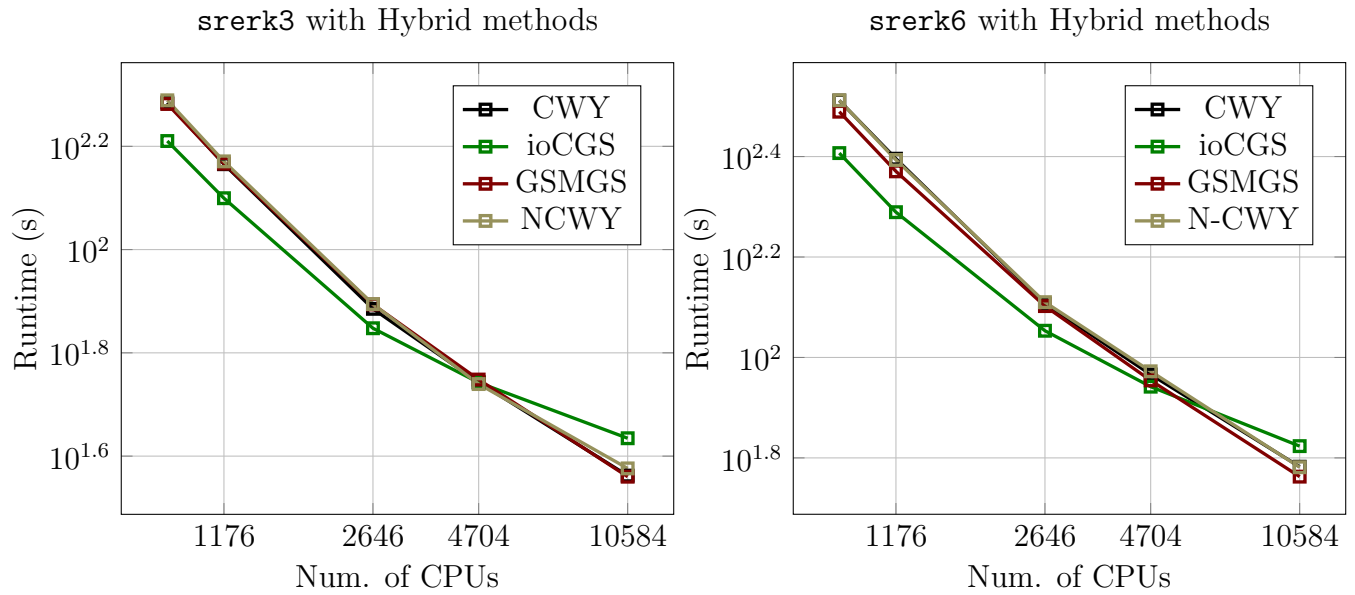


Figure 12: Strong scaling results for `srrerk3` and `srrerk6` with hybrid low-synchronization methods for SW-C5.

low-synchronization Method	p	EPI4	EPI5	EPI6	SRERK3	SRERK6
H-GSMGS	864	1.21	1.21	1.20	1.18	1.21
	1k	1.18	1.23	1.19	1.17	1.21
	2k	1.16	1.14	1.17	1.11	1.12
	4k	1.07	1.07	1.08	1.01	1.03
	10k	0.88	0.89	0.89	0.84	0.87
H-NCWY	864	1.22	1.20	1.19	1.20	1.27
	1k	1.16	1.21	1.16	1.18	1.27
	2k	1.11	1.08	1.09	1.11	1.14
	4k	1.02	1.02	1.00	0.99	1.07
	10k	0.86	0.85	0.86	0.87	0.91
H-CWY	864	1.20	1.20	1.19	1.19	1.27
	1k	1.19	1.21	1.16	1.16	1.28
	2k	1.11	1.07	1.09	1.09	1.13
	4k	1.03	1.06	1.01	1.00	1.06
	10k	0.86	0.85	0.88	0.85	0.91

Table 4: Runtime ratios of low-synchronization/ioCGS for SW-C5.

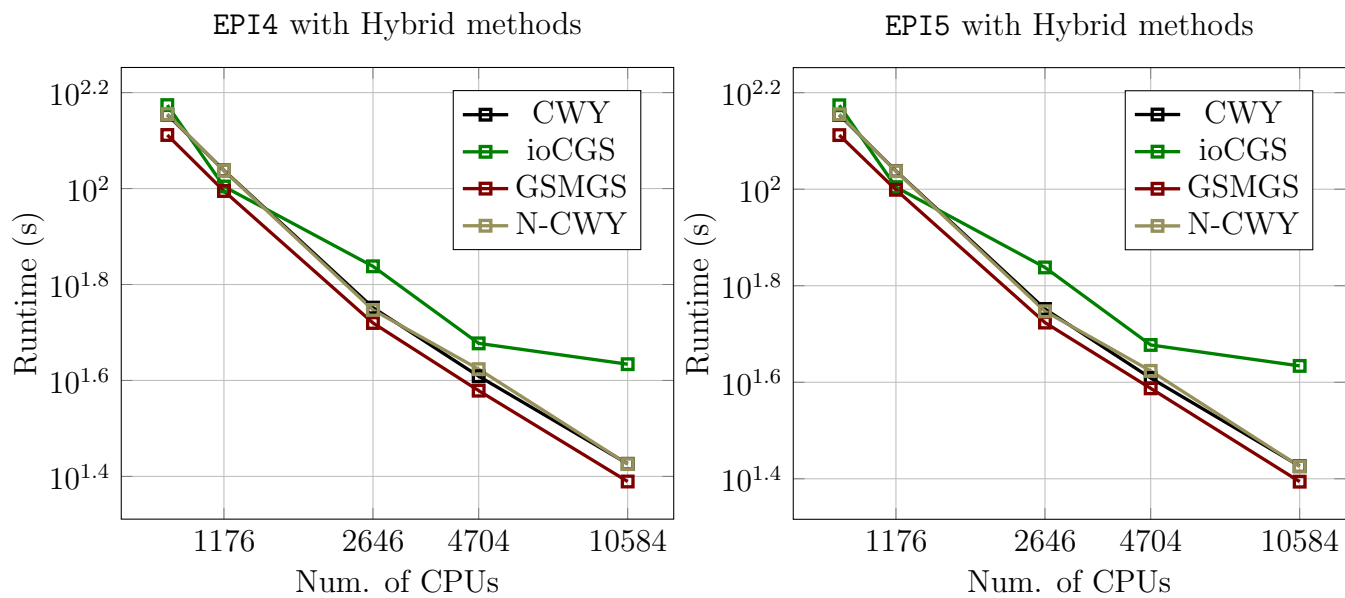


Figure 13: Strong scaling results for `epi4` and `epi5` with hybrid low-synchronization methods for SW-C6.

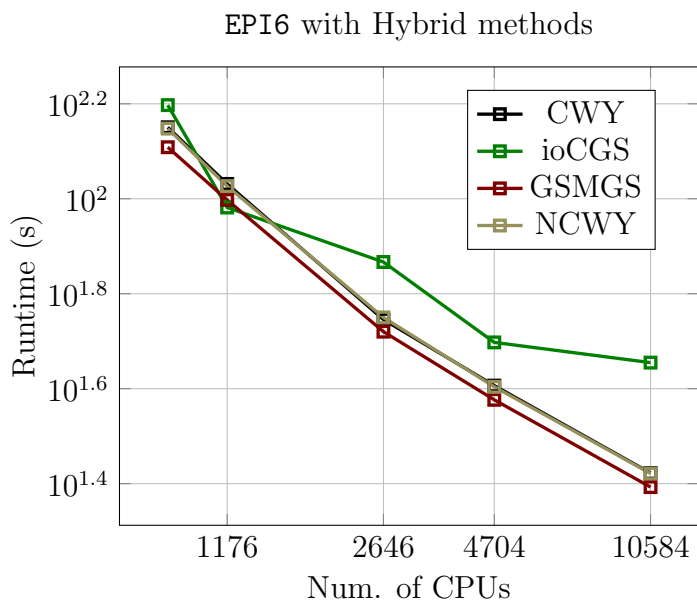


Figure 14: Strong scaling results for `epi6` with hybrid low-synchronization methods for SW-C6.

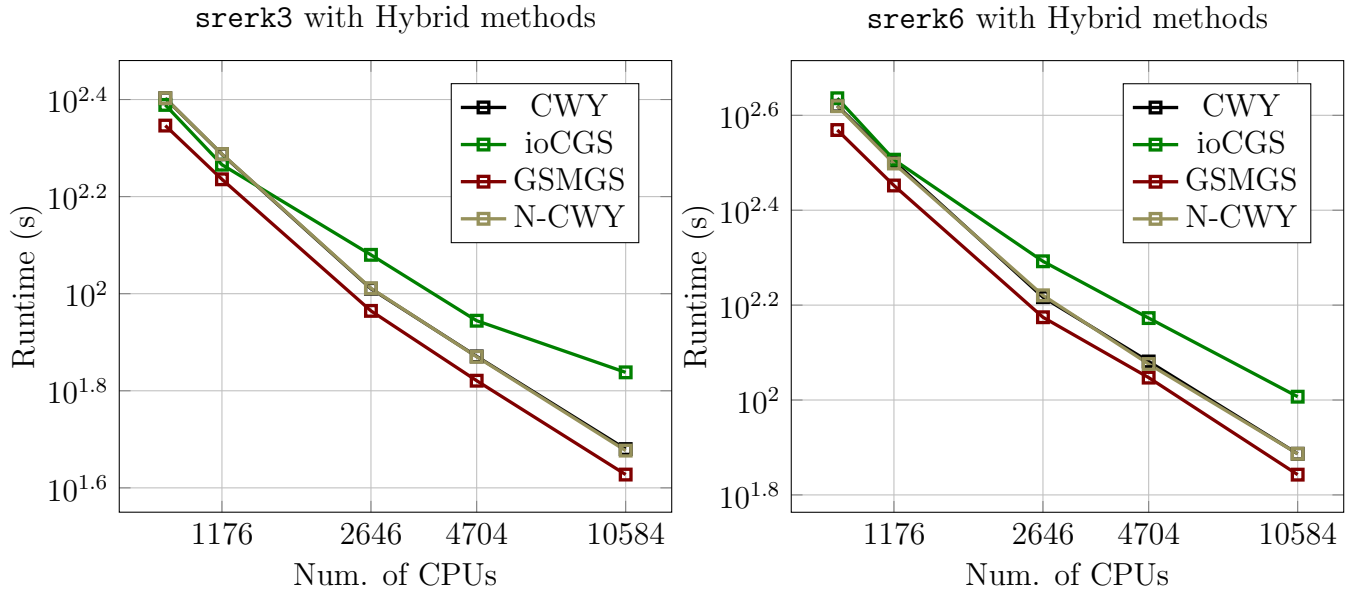


Figure 15: Strong scaling results for `srrerk3` and `srrerk6` with hybrid low-synchronization methods for SW-C6.

low-synchronization Method	p	EPI4	EPI5	EPI6	SRERK3	SRERK6
H-GSMGS	864	0.86	0.84	0.81	0.91	0.86
	1k	0.98	1.02	1.04	0.93	0.88
	2k	0.76	0.74	0.71	0.77	0.76
	4k	0.78	0.81	0.76	0.75	0.75
	10k	0.57	0.56	0.55	0.62	0.69
H-NCWY	864	0.96	0.92	0.89	1.03	0.96
	1k	1.08	1.10	1.11	1.05	0.98
	2k	0.81	0.80	0.76	0.85	0.85
	4k	0.88	0.84	0.81	0.84	0.80
	10k	0.62	0.60	0.58	0.69	0.76
H-CWY	864	0.96	0.92	0.90	1.03	0.96
	1k	1.08	1.11	1.12	1.05	0.99
	2k	0.82	0.80	0.76	0.85	0.84
	4k	0.85	0.85	0.81	0.84	0.81
	10k	0.62	0.60	0.59	0.69	0.76

Table 5: Runtime ratios of low-synchronization/ioCGS for SW-C6.

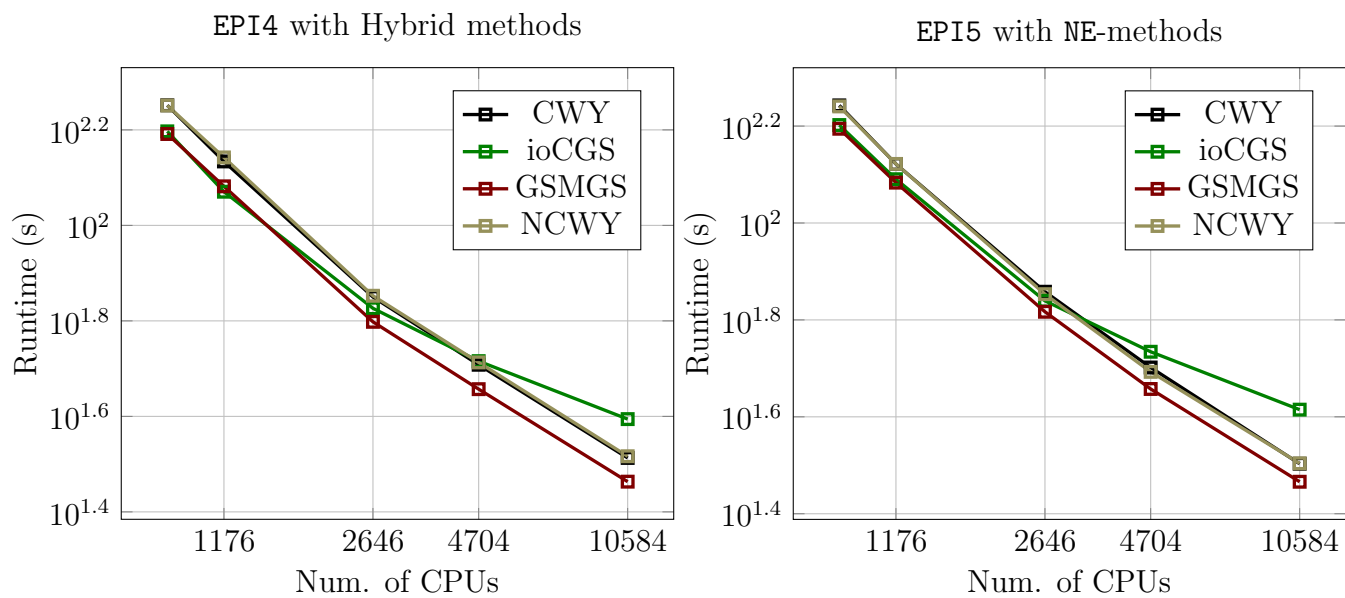


Figure 16: Strong scaling results for `epi4` and `epi5` with hybrid low-synchronization methods for SW-C8.

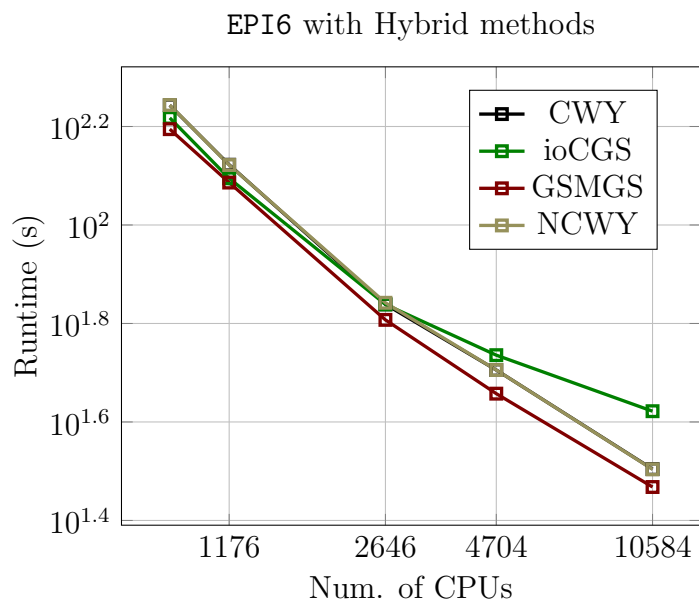


Figure 17: Strong scaling results for `epi6` with hybrid low-synchronization methods for SW-C8.

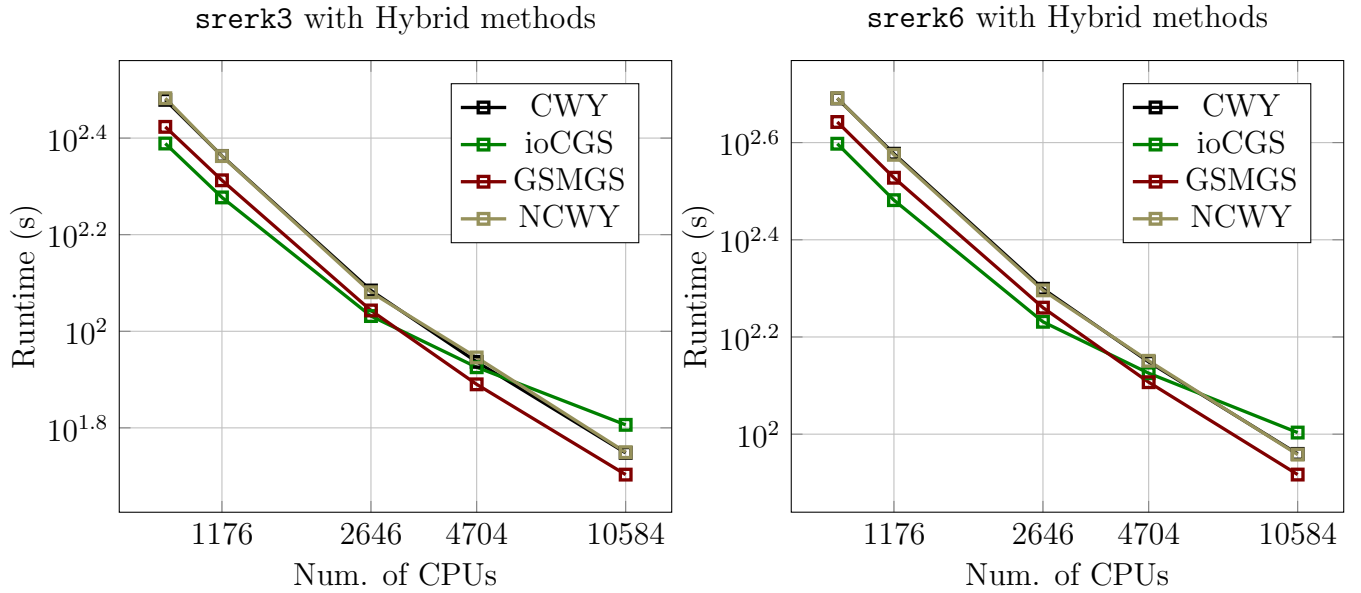


Figure 18: Strong scaling results for `srrerk3` and `srrerk6` with hybrid low-synchronization methods for SW-C8.

low-synchronization Method	p	EPI4	EPI5	EPI6	SRERK3	SRERK6
H-GSMGS	864	0.99	0.98	0.95	1.08	1.11
	1k	1.03	0.98	0.98	1.08	1.11
	2k	0.94	0.95	0.93	1.03	1.07
	4k	0.87	0.84	0.84	0.92	0.96
	10k	0.74	0.71	0.70	0.79	0.82
H-NCWY	864	1.13	1.09	1.06	1.24	1.24
	1k	1.18	1.08	1.06	1.22	1.24
	2k	1.06	1.03	1.01	1.12	1.16
	4k	0.99	0.91	0.93	1.05	1.06
	10k	0.84	0.77	0.76	0.88	0.90
H-CWY	864	1.13	1.10	1.06	1.23	1.24
	1k	1.16	1.07	1.07	1.22	1.25
	2k	1.06	1.04	1.00	1.13	1.17
	4k	0.98	0.93	0.93	1.03	1.05
	10k	0.83	0.77	0.76	0.87	0.90

Table 6: Runtime ratios of low-synchronization/ioCGS for SW-C8.

5 Conclusion

While Krylov projection-based algorithms are the methods of choice when a large scale stiff problem is integrated in time with an exponential integrator, the global synchronizations required to compute inner products at each Arnoldi iteration impose limitations on parallel scalability of such exponential-Krylov techniques. For example, using Modified Gram-Schmidt for the orthonalization

of the Krylov basis requires a significant number of global synchronizations that is proportional to the size of the Krylov subspace. In KIOPS, the Krylov subspace has to be recomputed at each substep $e^{\tau_i A} b_{\tau_i}$ (15b in sect. 2.2). Therefore, each substep relies on the Arnoldi iteration as the core component that determines the computational efficiency of exponential integrators. While incomplete orthogonalization can ameliorate this limitations for parallel implementation of an exponential integrator, many problems require full orthogonalization to be performed for reasons of accuracy and efficiency [50]. In this paper, we introduced full orthogonalization, hybrid low-synchronization MGS variants for the Krylov approximation of the matrix exponential for use inside an exponential integrators. These methods reduce the number of global synchronizations to one per Arnoldi-step independent of the Krylov dimension.

We studied performance of the new hybrid low-synchronization methods using a set of six test problems including three standard examples for testing stiff integrators and three problems that model different geophysical scenarios with the shallow water equations on the cubed-sphere grid. The numerical experiments confirmed the effectiveness of the low-synchronization approach for very large scale systems solved on massively parallel computing platforms. Exponential integrators with low-synchronization algorithms showed improved strong scalability with large numbers of processors in a CPU-only parallel environment. While the degree of improvement varied with the test cases and the integrators, the fact that the performance was improved for the largest number of processors remained consistent. The low-synchronization methods are designed for massively parallel systems such as multi-GPU implementations [51, 52], therefore it follows that the most improvement is seen with the largest processor size; $2k$ for sect. 4.3 and $10k$ for shallow water (sect. 4.4). Based on the results from the example problem in section 4.3, it is unclear which is the better low-synchronization algorithm to pair with exponential integrators. However, for the shallow water examples, specifically SW-C8 (fig. 16 - 18) and SW-C6 (fig. 13 - 15), the hybrid Iterated Gauß–Seidel MGS algorithm (H-GSMGS) (algorithm 4 and 7) had the greatest runtime improvements.

Although the numerical experiments compare an incomplete orthogonalization CGS and full orthogonalization MGS, the accuracy of each substep projection $e^{\tau_i A} b_{\tau_i}$ and the overall solution is not expected to improve. The adaptivity in the KIOPS algorithm for m_i and τ_i will ensure that at each substep the Krylov approximation $e^{\tau_i A} b_{\tau_i}$ has converged to the accuracy of the user-specified tolerance. However, with full-orthogonalization schemes, it is possible to have better substepping properties such as requiring less substeps. Therefore, in future work we aim to continue to improve the efficiency of the Krylov approximation by shifting towards the substepping procedure mentioned in section 2.2. For example, incorporating higher order adaptive time-stepping automatic controllers for τ such as proportional-integral (PI) or proportional-integral-derivative (PID) controllers based off of [47, 48, 24]. High-order adaptivity techniques for the substep size τ could lead to reducing the number of steps and/or the number of rejected steps. Refining the substepping procedure could lead to a further improvement in performance of exponential integrators.

6 Code availability

The code used to generate the results is available at: **create a repo with my branch of WX-factory**.

7 Acknowledgements

The origin of this study goes back to fruitful discussions with Stephen Thomas. Stimulating discussions with Kathryn Lund are also acknowledged. The authors are grateful to Vincent Magnoux for his assistance in running parallel simulations on the supercomputer which was crucial to the success of this study. This work was in part supported by a grant no. NSF-RTF-DMS-1840265 from the National Science Foundation, Computational Mathematics Program.

References

- [1] Awad H Al-Mohy and Nicholas J Higham. Computing the action of the matrix exponential, with an application to exponential integrators. *SIAM journal on scientific computing*, 33(2):488–511, 2011.
- [2] Thomas Ashby, Pieter Ghysels, W Heirman, and W Vanroose. The impact of global communication latency at extreme scales on Krylov methods. *Proceedings of the 12th International Conference on Algorithms and Architectures for Parallel Processing*, pages 428–442, 2012.
- [3] Peter W Bates, Sarah Brown, and Jianlong Han. Numerical analysis for a nonlocal Allen-Cahn equation. *Int. J. Numer. Anal. Model*, 6(1):33–49, 2009.
- [4] Daniel Bielich, Julien Langou, Stephen Thomas, Kasia Świrydowicz, Ichitaro Yamazaki, and Erik G Boman. Low-synch Gram–Schmidt with delayed reorthogonalization for Krylov solvers. *Parallel Computing*, page 102940, 2022.
- [5] Tommaso Buvoli. Exponential polynomial block methods. *SIAM Journal on Scientific Computing*, 43(3):A1692–A1722, 2021.
- [6] Tommaso Buvoli and Michael Minion. Exponential Runge-Kutta parareal for non-diffusive equations. *Journal of Computational Physics*, 497:112623, 2024.
- [7] Sara Calandrini, Konstantin Pieper, and Max D Gunzburger. Exponential time differencing for the tracer equations appearing in primitive equation ocean models. *Computer Methods in Applied Mechanics and Engineering*, 365:113002, 2020.
- [8] Marco Caliari, Fabio Cassini, and Franco Zivcovich. BAMPFI: Matrix-free and transpose-free action of linear combinations of φ -functions from exponential integrators. *Journal of Computational and Applied Mathematics*, 423:114973, 2023.
- [9] Marco Caliari, Peter Kandolf, Alexander Ostermann, and Stefan Rainer. The Leja method revisited: backward error analysis for the matrix exponential. *SIAM Journal on Scientific Computing*, 38(3):A1639–A1661, 2016.
- [10] Marco Caliari and Alexander Ostermann. Implementation of exponential rosenbrock-type integrators. *Applied Numerical Mathematics*, 59(3-4):568–581, 2009.
- [11] Valentin Dallerit. *Construction, analysis, and application of novel exponential time integrators for stiff problems*. PhD thesis, UC Merced, 2022.
- [12] Valentin Dallerit, Tommaso Buvoli, Mayya Tokman, and Stéphane Gaudreault. Second-order Rosenbrock-exponential (ROSEXP) methods for partitioned differential equations. *Numerical Algorithms*, pages 1–19, 2023.
- [13] Eric de Sturler and Henk A van der Vorst. Communication cost reduction for Krylov methods on parallel computers. In *International Conference on High-Performance Computing and Networking*, pages 190–195. Springer, 1994.
- [14] Florian De Vuyst. Efficient solvers for time-dependent problems: a review of IMEX, LATIN, PARAEXP and PARAREAL algorithms for heat-type problems with potential use of approximate exponential integrators and reduced-order models. *Advanced Modeling and Simulation in Engineering Sciences*, 3:1–14, 2016.

- [15] Pranab J Deka and Lukas Einkemmer. Exponential integrators for resistive magnetohydrodynamics: Matrix-free Leja interpolation and efficient adaptive time stepping. *The Astrophysical Journal Supplement Series*, 259(2):57, 2022.
- [16] Pranab J Deka, Lukas Einkemmer, and Mayya Tokman. Lexint: Package for exponential integrators employing Leja interpolation. *SoftwareX*, 21:101302, 2023.
- [17] Lukas Einkemmer, Mayya Tokman, and John Loffeld. On the performance of exponential integrators for problems in magnetohydrodynamics. *Journal of Computational Physics*, 330:550–565, 2017.
- [18] Richard A Friesner, Laurette S Tuckerman, Bright C Dornblaser, and Thomas V Russo. A method for exponential propagation of large systems of stiff nonlinear differential equations. *Journal of Scientific Computing*, 4:327–354, 1989.
- [19] Joseph Galewsky, Richard K Scott, and Lorenzo M Polvani. An initial-value problem for testing numerical models of the global shallow-water equations. *Tellus A: Dynamic Meteorology and Oceanography*, 56(5):429–440, 2004.
- [20] Efstratios Gallopoulos and Yousef Saad. Efficient solution of parabolic equations by Krylov approximation methods. *SIAM journal on scientific and statistical computing*, 13(5):1236–1264, 1992.
- [21] Stéphane Gaudreault, Martin Charron, Valentin Dallerit, and Mayya Tokman. High-order numerical solutions to the shallow-water equations on the rotated cubed-sphere grid. *Journal of Computational Physics*, 449:110792, 2022.
- [22] Stéphane Gaudreault, Greg Rainwater, and Mayya Tokman. KIOPS: A fast adaptive Krylov subspace solver for exponential integrators. *Journal of Computational Physics*, 372:236–255, 2018.
- [23] Pieter Ghysels, Thomas J Ashby, Karl Meerbergen, and Wim Vanroose. Hiding global communication latency in the GMRES algorithm on massively parallel machines. *SIAM journal on scientific computing*, 35(1):C48–C71, 2013.
- [24] Kjell Gustafsson, Michael Lundh, and Gustaf Söderlind. A PI stepsize control for the numerical solution of ordinary differential equations. *BIT Numerical Mathematics*, 28:270–287, 1988.
- [25] Vicente Hernández, José E Román, and Andrés Tomás. Parallel Arnoldi eigensolvers with enhanced scalability via global communications rearrangement. *Parallel Computing*, 33(7-8):521–540, 2007.
- [26] Marlis Hochbruck and Alexander Ostermann. Exponential integrators. *Acta Numerica*, 19:209–286, 2010.
- [27] Jianguo Huang, Lili Ju, and Yuejin Xu. A parareal exponential integrator finite element method for semilinear parabolic equations. *Numerical Methods for Partial Differential Equations*, page e23116, 2024.
- [28] Hung T Huynh. Discontinuous Galerkin via interpolation: the direct flux reconstruction method. *Journal of Scientific Computing*, 82(3):75, 2020.

- [29] Sun Kyung Kim and AT Chroropoulos. An efficient parallel algorithm for extreme eigenvalues of sparse nonsymmetric matrices. *The International Journal of Supercomputing Applications*, 6(1):98–111, 1992.
- [30] Dana A Knoll and David E Keyes. Jacobian-free Newton–Krylov methods: a survey of approaches and applications. *Journal of Computational Physics*, 193(2):357–397, 2004.
- [31] Antti Koskela. Approximating the matrix exponential of an advection-diffusion operator using the incomplete orthogonalization method. In *Numerical Mathematics and Advanced Applications-ENUMATH 2013*, pages 345–353. Springer, 2015.
- [32] Zbigniew Leyk. Breakdowns and stagnation in iterative methods. *BIT Numerical Mathematics*, 37:377–403, 1997.
- [33] John Loffeld. *Design, Implementation and Performance of Exponential Integrators for High Performance Computing Applications*. PhD thesis, UC Merced, 2013.
- [34] John Loffeld and Mayya Tokman. Comparative performance of exponential, implicit, and explicit integrators for stiff systems of ODEs. *Journal of Computational and Applied Mathematics*, 241:45–67, 2013.
- [35] Kathryn Lund. Adaptively restarted block Krylov subspace methods with low-synchronization skeletons. *Numerical Algorithms*, 93(2):731–764, 2023.
- [36] Cleve Moler and Charles Van Loan. Nineteen dubious ways to compute the exponential of a matrix, twenty-five years later. *SIAM review*, 45(1):3–49, 2003.
- [37] Jitse Niesen and Will M Wright. Algorithm 919: A Krylov subspace algorithm for evaluating the ϕ -functions appearing in exponential integrators. *ACM Transactions on Mathematical Software (TOMS)*, 38(3):1–19, 2012.
- [38] Pedro S Peixoto and Martin Schreiber. Semi-Lagrangian exponential integration with application to the rotating shallow water equations. *SIAM Journal on Scientific Computing*, 41(5):B903–B928, 2019.
- [39] Bernard Philippe and R Sidje. Parallel algorithms for the Arnoldi procedure. *Iterative Methods in Linear Algebra, II, IMACS Ser. Comput. Appl. Math*, 3:156–165, 1995.
- [40] Joshua D Romero. *On the development of the direct flux reconstruction scheme for high-order fluid flow simulations*. PhD thesis, Stanford University, 2017.
- [41] Axel Ruhe. Numerical aspects of Gram-Schmidt orthogonalization of vectors. *Linear algebra and its applications*, 52:591–601, 1983.
- [42] Yousef Saad. Variations on Arnoldi’s method for computing eigenelements of large unsymmetric matrices. *Linear algebra and its applications*, 34:269–295, 1980.
- [43] Yousef Saad. Krylov subspace methods for solving large unsymmetric linear systems. *Mathematics of computation*, 37(155):105–126, 1981.
- [44] Yousef Saad. Analysis of some Krylov subspace approximations to the matrix exponential operator. *SIAM Journal on Numerical Analysis*, 29(1):209–228, 1992.

- [45] Roger B Sidje. Alternatives for parallel Krylov subspace basis computation. *Numerical linear algebra with applications*, 4(4):305–331, 1997.
- [46] Roger B Sidje. Expokit: A software package for computing matrix exponentials. *ACM Transactions on Mathematical Software (TOMS)*, 24(1):130–156, 1998.
- [47] Gustaf Söderlind. Automatic control and adaptive time-stepping. *Numerical Algorithms*, 31:281–310, 2002.
- [48] Gustaf Söderlind. Digital filters in adaptive time-stepping. *ACM Transactions on Mathematical Software (TOMS)*, 29(1):1–26, 2003.
- [49] Gilbert W Stewart. *Matrix algorithms: volume 1: basic decompositions*. SIAM, 1998.
- [50] Jared Stewart, Mayya Tokman, Fabrizio Bisetti, Valentin Dallerit, and Oscar Diaz-Ibarra. Variable time-stepping exponential integrators for chemical reactors with analytical Jacobians. *arXiv preprint arXiv:2307.00136*, 2023.
- [51] Katarzyna Świrydowicz, Julien Langou, Shreyas Ananthan, Ulrike Yang, and Stephen Thomas. Low synchronization Gram–Schmidt and generalized minimal residual algorithms. *Numerical Linear Algebra with Applications*, 28(2):e2343, 2021.
- [52] Stephen Thomas, Erin Carson, Miro Rozložník, Arielle Carr, and Kasia Świrydowicz. Post-modern GMRES. *arXiv preprint arXiv:2205.07805*, 2022.
- [53] Stephen Thomas, Erin Carson, Miroslav Rozložník, Arielle Carr, and Katarzyna Świrydowicz. Iterated Gauss–Seidel gmres. *SIAM Journal on Scientific Computing*, pages S254–S279, 2023.
- [54] Stephen Thomas, Katarzyna Świrydowicz, Ruipeng Li, and Paul Mullaney. Neumann series in MGS-GMRES and Inner-Outer iterations. Technical report, National Renewable Energy Lab.(NREL), Golden, CO (United States), 2022.
- [55] Mayya Tokman. Efficient integration of large stiff systems of ODEs with exponential propagation iterative (EPI) methods. *Journal of Computational Physics*, 213(2):748–776, 2006.
- [56] Mayya Tokman, John Loffeld, and Paul Tranquilli. New adaptive exponential propagation iterative methods of Runge–Kutta type. *SIAM Journal on Scientific Computing*, 34(5):A2650–A2669, 2012.
- [57] Huy D Vo and Roger B Sidje. Approximating the large sparse matrix exponential using incomplete orthogonalization and Krylov subspaces of variable dimension. *Numerical linear algebra with applications*, 24(3):e2090, 2017.
- [58] David L Williamson, John B Drake, James J Hack, Rüdiger Jakob, and Paul N Swarztrauber. A standard test set for numerical approximations to the shallow water equations in spherical geometry. *Journal of computational physics*, 102(1):211–224, 1992.
- [59] Ichitaro Yamazaki, Stephen Thomas, Mark Hoemmen, Erik G Boman, Katarzyna Świrydowicz, and James J Elliott. Low-synchronization orthogonalization schemes for s-step and pipelined krylov solvers in trilinos. In *Proceedings of the 2020 SIAM Conference on Parallel Processing for Scientific Computing*, pages 118–128. SIAM, 2020.